The decrotonylase FoSir5 facilitates mitochondrial metabolic state switching in conidial germination of *Fusarium oxysporum*

Ning Zhang[1,†], Limin Song[1,†], Yang Xu[1], Xueyuan Pei[2], Ben F. Luisi[2], Wenxing Liang[1,*]

[1] Key Lab of Integrated Crop Pest Management of Shandong Province, College of Plant Health and Medicine, Qingdao Agricultural University, Qingdao, China

[2] Department of Biochemistry, University of Cambridge, Cambridge, UK

[†] N.Z. and L.S. contributed equally to this work.

[*]For correspondence: wliang1@qau.edu.cn

Abstract

Fusarium oxysporum is one of the most important pathogenic fungi with a broad range of plant and animal hosts. The first key step of its infection cycle is conidial germination, but there is limited information available on the molecular events supporting this process. We show here that germination is accompanied by a sharp decrease in expression of FoSir5, an ortholog of the human lysine deacetylase SIRT5. We observe that FoSir5 decrotonylates a subunit of the fungal pyruvate dehydrogenase complex (FoDLAT) at K148, resulting in inhibition of the activity of the complex in mitochondria. Moreover, FoSir5 decrotonylates histone H3K18, leading to a downregulation of transcripts encoding enzymes of aerobic respiration pathways. Thus, the activity of FoSir5 coordinates regulation in different organelles to steer metabolic flux through respiration. As ATP content is positively related to fungal germination, we propose that FoSir5 negatively modulates conidial germination in *F. oxysporum* through its metabolic impact. These findings provide insights into the multifaceted roles of decrotonylation, catalysed by FoSir5, that support conidial germination in *F. oxysporum*.

Introduction

Fusarium oxysporum is a transkingdom pathogen known to infect more than 100 plant species (Michielse & Rep, 2009) and immune-compromised patients (Nucci & Anaissie, 2007). Therefore, it is of great importance to gain insight into the molecular processes involved in pathogenesis of this fungus. *F. oxysporum* invades roots and can cause wilt diseases through colonization of xylem tissue. Fungal conidia are the first structures that the host immune system encounters during infection, and conidial germination is a crucial step for *F. oxysporum* infection. The early initiation stage of conidial germination represents a critical point to inhibit fungal growth and counter pathogenic infection (Deng, Yang et al., 2015). However, the molecular mechanism by which *F. oxysporum* regulates its germination process remains largely unknown.

Lysine acetylation, one of the most common post-translational modifications (PTMs), is involved in regulation of conidial germination in plant-associated fungi (Dubey, Lee et al., 2019, Wang, Cai et al., 2018, Zhang, Yang et al., 2020b). In recent decades, besides acetylation, numerous other short-chain acylation modifications have been discovered on lysine (K) residues, including crotonylation, malonylation, succinylation, propionylation, glutarylation, and butyrylation (Chen, Sprung et al., 2007, Hirschey & Zhao, 2015, Kim, Sprung et al., 2006, Park, Chen et al., 2013, Tan, Luo et al., 2011b, Tan, Peng et al., 2014b). Among them, lysine crotonylation (Kcr), first identified on histones, is also able to target other proteins involved in various cellular processes (Wei, Mao et al., 2017b, Wu, Li et al., 2017, Xu, Wan et al., 2017). Kcr is recognized by histone-binding “reader” modules, including AF9 YEATS,

YEATS2, MOZ and DPF2, in a type- and site-specific manner (Li, Sabari et al., 2016, Xiong, Panchenko et al., 2016, Zhao, Guan et al., 2016). Histone crotonylation by p300 has been shown to promote transcription *in vitro* and manipulating cellular concentration of crotonyl-CoA affects gene expression (Sabari, Tang et al., 2015). Although a recent proteomic analysis reveals that Kcr is tightly associated with virulence of the necrotrophic fungus *Botrytis cinerea* (Zhang, Yang et al., 2020a), it is not clear whether this modification is involved in the regulation of fungal germination.

Previous studies have identified histone deacetylase SIRT1 as being responsible for the removal of crotonylation in the nucleus (Bao, Wang et al., 2014, Feldman, Baeza et al., 2013, Wei, Liu et al., 2017a). The NAD^+-dependent sirtuins (SIRTs) have an expanded repertoire of deacylase activities and display widespread subcellular distributions (Bell & Guarente, 2011, Cen, Y Youn et al., 2011, Kanfi, Naiman et al., 2012). Three mammalian sirtuins (SIRT3, SIRT4 and SIRT5) localize mostly or exclusively to the mitochondrial matrix, the powerhouse of the cell producing the bulk of cellular ATP through oxidative phosphorylation (Ryan, 2018). SIRT3 is considered the major deacetylase of mitochondria (Lombard, Alt et al., 2007), while SIRT4 mainly functions as a lipoamidase that regulates pyruvate dehydrogenase complex activity (Mathias, Greco et al., 2014). SIRT5, which possesses poor deacetylase activity (Du, Zhou et al., 2011), preferentially regulates the levels of lysine succinylation, malonylation, and glutarylation, playing multiple roles in regulating different metabolic pathways including glycolysis/gluconeogenesis, fatty

acid β-oxidation, oxidative phosphorylation, the urea cycle, and ketogenesis (Hirschey & Zhao, 2015, Park et al., 2013, Tan, Peng et al., 2014a). However, no information on the regulation of crotonylation in mitochondria is available.

The SIRTs are also present in filamentous fungi and control a variety of cellular processes (Haigis & Sinclair, 2010). Seven SIRTs, NST-1 to NST7, have been identified in *Neurospora crassa*, which mediate telomeric silencing in this fungus (Smith, Kothe et al., 2008). In *Podospora anserina*, deletion of *PaSir2* resulted in a significant reduction of cell life span (Boivin, Gaumer et al., 2008). The sirtuins, HstD in *Aspergillus oryzae* and sirtuin A in *A. nidulans*, control secondary metabolite production (Itoh, Shigemoto et al., 2017, Kawauchi, Nishiura et al., 2013). However, except for the characterization of *Magnaporthe oryzae MoSir2* in biotrophic growth in host rice plants (Fernandez, Marroquin-Guzman et al., 2014), relatively little is known about the function of SIRTs in plant pathogens.

In this study, we show that the *F. oxysporum* FoSir5, an ortholog of the human lysine deacetylase, possesses decrotonylase activities *in vitro* and *in vivo*. In mitochondria, FoSir5 interacts with and removes the crotonyl group from the E2 component dihydrolipoyllysine acetyltransferase (FoDLAT) of the pyruvate dehydrogenase complex (PDC), the activity of which links glycolysis to the tricarboxylic acid (TCA) cycle. The specific decrotonylation of K148 of FoDLAT by FoSir5 leads to decreased PDC activity and acetyl-CoA generation. FoSir5 is also distributed in nuclei, where it directly regulates the enrichment of crotonylated H3K18 (H3K18cr) on genes involved in the TCA cycle and electron transport chain

(ETC) pathways. The integrated regulation by FoSir5 in different organelles represses mitochondrial ATP biosynthesis, impeding fungal conidial germination. Importantly, we find that by decreasing the expression of *FoSir5*, *F. oxysporum* increases the ATP supply that supports the energy consumption demands of germination, emphasizing the importance of this regulatory process. These findings provide a clear example in which plant pathogenic fungi control conidial germination through an exquisite regulatory network that links metabolic activity to the developmental program of infection.

Results

FoSir5 has both mitochondrial and extra-mitochondrial decrotonylase activity in *vitro*

Members of the sirtuin family lysine deacetylases (KDACs) exhibit various subcellular localizations and are distributed in the nucleus, cytoplasm, and mitochondria (North & Verdin, 2004). However, none of the sirtuin KDACs in *F. oxysporum* have yet been characterized. The *F. oxysporum* genome contains seven genes predicted to encode a protein with the NAD^+-dependent deacetylase domain typical of the sirtuin KDACs, the same number found in the genomes of human and the fungus *N. crassa* (Michishita, Park et al., 2005, Smith et al., 2008). We designated these genes *FoSir1* to *FoSir7* (Figure 1A).

The *FoSir5* (FOXG_05932) gene encodes a 298-amino acid protein that is predicted partition to the fungal mitochondrion (using WoLF PSORT). Similar to NST-6 (Smith et al., 2008), FoSir5 was identified as the closest homolog to human mitochondria-localized SIRT5 (Figure 1B). To confirm the subcellular localization of FoSir5, *FoSir5* cDNA was fused with green fluorescent protein (GFP) and transformed into *F. oxysporum*. As shown in Figure 1C, GFP-tagged FoSir5 partially colocalized with a mitochondrial fluorophore, and a detectable FoSir5 fraction was also present outside the organelle in the cytosol. Consistent with the confocal microscopy results, subcellular fractionation revealed that a significant fraction of FoSir5-GFP was present in the mitochondrion and cytosol (Figure 1D). The analysis also reveals a small fraction of FoSir5 in the nuclear fraction. Like *F. oxysporum*

FoSir5, the human ortholog SIRT5 is also found both inside and outside the mitochondrion (Rardin, He et al., 2013).

Three human sirtuins, SIRT1-SIRT3, were recently suggested to remove crotonyl groups from histones *in vitro* (Bao et al., 2014). To investigate whether the FoSir5 protein possesses similar activity, we incubated bacterially expressed and purified recombinant FoSir5 with native calf thymus histones (CTH) in the presence of crotonyl-CoA. The pan anti-Kcr antibody specifically recognizing crotonylated lysine residues (Liu, Yu et al., 2017, Tan, Luo et al., 2011a) was used for Western Blotting to detect Kcr signal. Histone Kcr was detected in the untreated CTH samples, in agreement with earlier studies (Sabari et al., 2015), and the addition of FoSir5 resulted in a decrease in histone Kcr (Figure 1E), indicating that FoSir5 is able to remove crotonyl groups from histones *in vitro*.

To investigate whether *FoSir5* is involved in regulating *F. oxysporum* growth, we assessed the expression of the gene during different growth phases by quantitative real-time PCR (qRT-PCR). As shown in Figure 1F, the expression of *FoSir5* was high in the conidia, decreased dramatically during the germination process (4-12 h), and then recovered in the mycelium at 24 h. These differential expression patterns suggest that *FoSir5* might play a role in the conidial germination of *F. oxysporum*.

FoSir5 modulates PDC activity by decrotonylating the E2 component of PDC

Since a large proportion of FoSir5 was localized in the mitochondria, we explored whether FoSir5 is involved in the decrotonylation of mitochondrial proteins in *F.*

177 *oxysporum*. For this purpose, we utilized the FoSir5-GFP transformant and performed
178 immunoprecipitation followed by LC-MS/MS. Among the candidate binding partners
179 (Supplementary File 1), the E2 component of the pyruvate dehydrogenase complex,
180 FoDLAT, a putative mitochondrial protein (FOXG_11462), was selected for further
181 analysis.

182 Fluorescence observation verified the expected mitochondrial localization of
183 FoDLAT in *F. oxysporum* (Figure 2-figure supplement 1A). FoSir5-GFP and
184 FoDLAT-Flag fusion constructs were co-introduced into *F. oxysporum* protoplasts,
185 and positive transformants were selected. FoDLAT was detected in the proteins that
186 eluted from anti-GFP beads using the anti-Flag antibody, suggesting that FoDLAT
187 interacts with FoSir5 (Figure 2A). This interaction was also confirmed by *in vitro*
188 pull-down assay, indicating a direct interaction between the two proteins (Figure 2B).

189 To test whether FoSir5 decrotonylates FoDLAT, we first generated ΔFoSir5
190 deletion mutants by replacing the coding region with the hygromycin resistance
191 cassette and FoSir5 overexpression strains fused with a C-terminal Flag tag driven by
192 the strong constitutive promoter RP27. A total of 3 transformants from each group
193 were obtained (Figure 2-figure supplement 2). The transformants from all groups had
194 the same phenotypes, although only data for the mutant strain ΔFoSir5.3 (ΔFoSir5)
195 and the overexpression strain FoSir5-Flag-1 (OE-1) are presented below. Then, we
196 transformed and expressed FoDLAT-GFP in the Fo, ΔFoSir5 and OE-1 strains. The
197 crotonylation levels of immunoprecipitated FoDLAT were then tested. Compared with
198 that in the Fo strain, we found markedly increased crotonylation of FoDLAT in

ΔFoSir5 (Figure 2-figure supplement 3). These data indicated that FoSir5 is responsible for the decrotonylation of FoDLAT. Although SIRT5 was reported to possess robust demalonylase, desuccinylase and deglutarylase activities in mammals (Hirschey & Zhao, 2015, Park et al., 2013, Tan et al., 2014a), our results showed that FoSir5 had no detectable impact on succinylation, malonylation, or glutarylation of the FoDLAT protein in *F. oxysporum* (Figure 2-figure supplement 3).

To determine the crotonylation sites of FoDLAT, we purified the FoDLAT-GFP fusion protein from *F. oxysporum* and identified by mass spectrometry lysine 148 as a site of modification (Figure 2-figure supplement 1B). To further confirm whether K148 is crotonylated *in vivo*, we mutated lysine 148 to arginine (R) or glutamine (Q), respectively, and developed a specific antibody against crotonylated K148 of FoDLAT (anti-K148cr-FoDLAT) to examine their crotonylation. Note that arginine and glutamine mimic non-acylated and acylated lysine, respectively, with respect to charge on the residues (Sun, Xu et al., 2020, Yu, Bu et al., 2020). The Western analyses detected signals with only the wild-type (WT) FoDLAT but not the Q and R mutants, indicating that K148 is indeed crotonylated *in vivo*. We also found that inactivation and overexpression of FoSir5 led to significantly increased and decreased K148 crotonylation of WT FoDLAT, respectively (Figure 2C and D). To further verify that FoSir5 plays a role in the decrotonylation of FoDLAT, an *in vitro* decrotonylation assay was performed using recombinant proteins purified from *E. coli*. The results showed that K148 crotonylation has also occurred on FoDLAT in *E. coli* and addition of FoSir5 in the presence of NAD^+ reduced K148 crotonylation of WT FoDLAT but

not the Q form (Figure 2E). These data demonstrate that FoSir5 is responsible for K148 decrotonylation of FoDLAT.

To explore how this crotonylation site might affect FoDLAT function, we first generated a homology model of the fungal enzyme based on the crystal structure of the homologous human E2. In the PDC assembly, E2 is the dihydrolipoyl acetyltransferase component, and comprises a biotin-lipoyl domain, an interaction domain that binds the dihydrolipoyl dehydrogenase (E3) component, and the catalytic domain. The crotonylation site maps to an intradomain linker that is predicted to be flexible (Figure 2-figure supplement 1C and D). The flexibility enables the biotin-lipoyl domain to shuttle substrates between the E1 and E2 catalytic sites and then to the E3 site for an oxidation step. Given that DLAT is likely an essential component of PDC function (no DLAT deletion mutants could be obtained after numerous attempts in this research), we examined the impact of changed FoSir5 levels on the endogenous cellular activity of the PDC. PDC activity was elevated in the ΔFoSir5 strain and reduced in the OE-1 strain compared with the Fo and the complemented strain ΔFoSir5-C (Figure 2F). To further determine whether the crotonylation site of FoDLAT plays a role in PDC function, we detected PDC activity in the K148 mutant strains. As shown in Figure 2F, the K148Q and K148R mutant strains demonstrated increased and decreased PDC activity, respectively. Furthermore, the levels of acetyl-CoA, a direct product of E2 catalytic activity, followed a pattern similar to that of PDC activity among the different strains (Figure 2G). Collectively, these data establish a specific and prominent role of FoSir5 in FoDLAT

243 decrotonylation and PDC enzymatic inactivation.

244

245 **FoSir5 directly regulates the expression of genes related to aerobic respiration**
246 **through H3K18 decrotonylation**

247 Subcellular fractionation showed a small portion of FoSir5 in the nuclei, and FoSir5
248 could remove crotonyl groups from histones *in vitro* (Figure 1C-E). This finding lead
249 us to explore whether FoSir5 regulates histone Kcr in cells. As shown in Figure 3A,
250 FoSir5 inactivation caused the accumulation of H3K18cr, but has little effect on
251 H3K18ac or H3K9cr. Therefore, we performed RNA-seq analysis to detect transcripts
252 that might be regulated by FoSir5 in *F. oxysporum*. Three biological replicates
253 consisting of mRNA isolated from the Fo and ΔFoSir5 mutant strains were assessed,
254 identifying 1566 up- and 856 downregulated (fold change > 2, $P < 0.05$) genes in the
255 ΔFoSir5 compared with the Fo strain (Supplementary File 2). Given the function of
256 histone decrotonylases (HDCRs) in gene repression and H3K18cr in gene activation
257 (Sabari et al., 2015), we hypothesized that the target genes of FoSir5 were likely
258 among the upregulated genes. Gene Ontology (GO) functional annotation and KEGG
259 pathway analysis of those upregulated genes revealed significant enrichment of their
260 products in the TCA cycle, ETC and ATP synthesis (Figure 3-figure supplement 1).
261 We selected for experimental validation eight upregulated genes related to types of
262 energy metabolism, namely *NDHB1* (NADH-quinone oxidoreductase chain B 1),
263 *MDH* (malate dehydrogenase), *CYC1* (cytochrome C1), *IDH2* (isocitrate
264 dehydrogenase subunit 2), *SDH* (succinate dehydrogenase), *ATP5H* (ATP synthase D

chain), *NDH8* (NADH dehydrogenase iron-sulfur protein 8), and *CYBS* (succinate dehydrogenase cytochrome b small subunit) (Figure 3B). qRT-PCR analysis indicated that all of the 8 genes were indeed upregulated in the ΔFoSir5 strain and downregulated in the OE-1 strain compared with the Fo and ΔFoSir5-C strains (Figure 3C).

To determine whether FoSir5 directly regulates these 8 genes, a chromatin immunoprecipitation (ChIP) qPCR assay was performed using a GFP antibody. Primers in promoter regions near putative transcription start sites (TSSs) were designed to evaluate the enrichment of FoSir5-GFP in the 8 energy metabolism-related genes. The results showed that these regions were highly enriched by FoSir5 in the FoSir5-GFP strain compared with the Fo strain (Figure 3D). To test whether these promoter regions are also H3K18 crotonylation locations in genomic DNA, we further performed ChIP using an anti-H3K18cr antibody, followed by qPCR. As shown in Figure 3E, these regions were also enriched by H3K18cr in the ΔFoSir5 compared with the Fo strain. *FoACTIN* was used as a negative control which was not enriched by anti-GFP or anti-H3K18cr (Figure 3D and E). Overall, these observations demonstrated that FoSir5 and H3K18cr were enriched in the promoter regions of 8 energy-related genes, indicating that FoSir5 and H3K18cr participate in the transcriptional regulation of metabolic energy-generating systems in *F. oxysporum*.

FoSir5 represses ATP synthesis in germinating *F. oxysporum*

Most intracellular ATP comes from the oxidation of glucose-derived pyruvate by the

TCA cycle and oxidation of NADH in mitochondria via the ETC. As genes involved in mitochondrial ATP synthesis were directly regulated by FoSir5, we speculated that change of FoSir5 level will result in altered ATP content. As shown in Figure 4A-E, dramatic decrease of FoSir5 during germination led to reduced decrotonylase activity of this enzyme, and as a result, the K148 crotonylation of FoDLAT, PDC activity, acetyl-CoA generation, H3K18cr level and expression of the 8 energy-related genes were elevated. Meanwhile, declined enrichment of FoSir5 in promoter regions of these genes was observed (Figure 4F). Ultimately, the ATP content was elevated during the germinating process (Figure 4G). Consistent with these observations, inactivation of FoSir5 increased the level of ATP by ~70%, whereas overexpression of this enzyme significantly decreased ATP content in germinating conidia at 8 h post incubation (Figure 4H). Moreover, the FoSir5 mutant and overexpression strains exhibited a continuous high and low level of ATP during the whole germinating process, respectively (Figure 4-figure supplement 1), further confirming the relationship between FoSir5 and ATP.

FoSir5 affects conidial germination of *F. oxysporum* by modulating ATP generation

Previous studies demonstrated that ATP plays a significant role in energizing cellular developmental processes (Wang, Mei et al., 2013). As conidial germination is of high energy-consumption, it is reasonable to envision that elevated ATP level benefits this process. Therefore, we determined germination rates of conidia treated with

exogenous ATP at different concentrations from 0 μM to 50 μM. Not unexpectedly, supply with at least 10 μM ATP increased germination rate of *F. oxysporum* conidia by about 50% (Figure 5A).

Modulation of ATP levels of *F. oxysporum* to support germination is likely to involve an extensive regulatory network, and the sharp decline of FoSir5 during germination (Figure 1F) might be expected to be important for this process. To examine this point in more detail, we tested conidial germination of Fo, ΔFoSir5 and ΔFoSir5-C mutant strains. We found that while inactivation of FoSir5 elevated conidial germination, reintroduction of FoSir5 recovered the phenotype of the WT strain. Conversely, overexpression of FoSir5 to mimic dysregulation of its decline led to obviously decreased germination (Figure 5B and C). Addition of exogenous ATP completely rescued the impeded germination of the OE-1 strain (Figure 5D), confirming an important role of ATP in conidial germination. In support of these observations, either K148Q mutation of FoDLAT or overexpression of key genes of the TCA cycle and ATP metabolism including *MDH*, *ATP5H* and *CYC1* (Figure 5-figure supplement 1), led to elevated ATP and conidial germination, whereas the K148R mutant strain demonstrated decreased ATP level and germination (Figure 5E and F). Taken together, all of these data strongly suggest a crucial role for FoSir5 in conidial germination through modulating ATP generation.

Based on these results and those presented above, we propose a simple model to explain how FoSir5 modulates conidial germination of *F. oxysporum* (Figure 6). In mitochondria, FoSir5 binds and decrotonylates FoDLAT at K148, and this

modification inhibits the enzymatic activity of PDC leading to reduced production of acetyl-CoA. At the same time, FoSir5-catalyzed H3K18cr decrotonylation in the nucleus transcriptionally represses the expression of genes participating in the TCA cycle and ETC pathways with acetyl-CoA being the initial substrate. Consequently, the coordinated regulation by FoSir5 in different organelles results in the repression of mitochondrial ATP synthesis. During conidial germination, by decreasing FoSir5 level, *F. oxysporum* eliminates inhibition of ATP metabolism essential for this process.

FoSir5 is required for full virulence of *F. oxysporum* on tomato

To determine whether FoSir5-mediated ATP metabolism affects pathogenicity of *F. oxysporum*, infection assays were performed by dipping the roots of 2-week-old tomato seedlings in conidial suspension of the Fo, ΔFoSir5, ΔFoSir5-C, and OE-1 strains. In our repeated experiments, compared with Fo and ΔFoSir5-C, the ΔFoSir5 strain exhibited higher infection ability, whereas overexpression of *FoSir5* reduced disease development by ~40% (Figure 4-figure supplement 2A and B). To determine whether altered level of FoSir5 affected *in planta* fungal growth, we quantified fungal biomass in roots by analyzing the expression level of *F. oxysporum FoEF-1α* as an indicator. Consistent with the results of infection assays, the level of *FoEF-1α* in ΔFoSir5 inoculated plants increased almost 2-fold, and the amount of fungal transcript was reduced by ~70% in OE-1 infected roots (Figure 4-figure supplement 2C). These results indicate that FoSir5 exerts a negative effect on virulence of *F. oxysporum*, and the increased and decreased pathogenicity of ΔFoSir5 and OE-1,

353 respectively, is likely due to increased and decreased germination rates.

354

355

356

357

358

359

360

361

362

363

364

365

366

367

368

369

370

371

372

373

374

Discussion

Lysine crotonylation, a newly discovered post-translational modification reversibly controlled by lysine crotonytransferases and decrotonylases, is involved in numerous cellular processes, including chromatin remodelling, metabolism, protein folding and the cell cycle (Wan, Liu et al., 2019, Wei et al., 2017b, Xu et al., 2017). Although a growing number of crotonylated proteins have been identified in multiple organisms (Kwon, Kim et al., 2018, Liu, Xue et al., 2018, Sun, Liu et al., 2017, Sun, Qiu et al., 2019, Wei et al., 2017b, Zhang et al., 2020a), the enzymes responsible for lysine crotonylation and their physiological role remain poorly defined, especially for the decrotonylation of non-histone proteins. The information presented here indicates that a sirtuin family protein, FoSir5, functions as a lysine decrotonylase to modulate conidial germination in *F. oxysporum*. As such, these findings greatly expand our understanding of lysine decrotonylases and open up new possibilities for further investigations of the regulatory role of these enzymes.

The studies described here provide evidence that FoSir5 can modulate ATP synthesis through lysine decrotonylation in different organelles and thus conidial germination of *F. oxysporum*. Specifically, we found that (i) FoSir5 is distributed in different cellular compartments and possesses lysine decrotonylase activity; (ii) in mitochondrion, FoSir5 removes a crotonyl group from the K148 residue of FoDLAT, and therefore inhibits PDC activity and acetyl-CoA production; (iii) in the nucleus, FoSir5 represses the expression of genes associated with aerobic respiration by decrotonylating H3K18cr; (iv) the coordinated regulation by FoSir5 in the

mitochondrion and nucleus impacts on ATP synthesis; (v) ATP content is positively associated with conidial germination; and (vi) *F. oxysporum* downregulates *FoSir5* level during germination to elevate ATP level required for this process. These findings indicate that fungal pathogens employ an elaborate mechanism to carefully control energy metabolism. The mechanism by which FoSir5 is downregulated during germination is a topic to be explored in future studies, but it is clear that this complex regulatory system serves as a salient example of how eukaryotes can control their development through regulating the action of a lysine decrotonylase.

Sirtuins are class III KDACs that require NAD for their deacylation activities. Seven sirtuin isoforms (SIRT1 to SIRT7) are expressed in mammalian cells. These isoforms display widespread subcellular distributions, as SIRT1, SIRT6 and SIRT7 are nuclear, SIRT2 is predominantly cytoplasmic, and SIRTs3-5 are mitochondrial (Gertz & Steegborn, 2016, Michishita et al., 2005). Recent studies have shown the both mitochondrial and extra-mitochondrial localization of SIRT5 (Park et al., 2013), while SIRT1 and SIRT2 can accumulate in the cytosol and nucleus, respectively, under specific circumstances (Byles, Chmilewski et al., 2010, Vaquero, Scher et al., 2006). However, the synergistic action of sirtuins among different organelles is poorly characterized. Our findings that SIRT5 simultaneously act on histones in chromatin and enzymes in the mitochondria to modulate ATP generation provide a clear example of coordinated functions of one sirtuin protein in different cellular compartments. With the identification of more lysine deacylases in future research, it is likely that the findings reported here are only the beginning of what will be a widespread

419 phenomenon in eukaryotes.

420 By converting pyruvate to acetyl-CoA, PDC is an important gatekeeper that links
421 glycolysis to the TCA cycle and oxidative phosphorylation. Therefore, controlling the
422 activity of this enzyme complex impacts on metabolic flux and the efficiency of ATP
423 generation. In mammalian cells, pyruvate dehydrogenase phosphatases
424 dephosphorylate the E1α subunit and activate the PDC, while SIRT5-mediated
425 desuccinylation of PDC subunits, including mainly E1α, E1β and E3, suppresses PDC
426 activity (Park et al., 2013). The data described here provide evidence that FoSir5
427 decrotonylates the E2 subunit of the PDC at K148 and thus inhibits PDC activity in *F.*
428 *oxysporum*. All these findings indicate that cells employ a variety of approaches to
429 tightly regulate the activity of PDC. It will be of considerable interest to examine the
430 coordinated effect exerted by different modifications in future studies.

431 Conidia are reproductive structures important for both dispersal and survival
432 within harsh environments. In this study, we found that the expression level of *FoSir5*
433 was higher in conidia than in other growth stages (Figure 1F), indicating that
434 inhibition of mitochondrial ATP biosynthesis by FoSir5 may be helpful for
435 maintaining low energy expenditure of conidia under unsuitable conditions.
436 Thereafter, during the germination process needing high energy consumption, the
437 expression of *FoSir5* sharply declined, resulting in enough ATP production to support
438 breaking dormancy and the formation of a germ tube. Then, *FoSir5* levels were
439 restored to a higher level in the mycelium, likely to control energy metabolism
440 properly. Given the fact that conidial germination is crucial for infection and there is

441 limited information on the regulation of this process (Deng et al., 2015, Leroch,
442 Kleber et al., 2013, Sharma, Sengupta et al., 2016), our findings that deletion of
443 FoSir5 resulted in enhanced pathogenicity provide candidate target proteins for
444 exploring new effective fungicides against *F. oxysporum* and other plant pathogens.
445
446
447
448
449
450
451
452
453
454
455
456
457
458
459
460
461
462

Materials and methods

Fungal strains and culture conditions

F. oxysporum f. sp. *lycopersici* strain 4287 (Fo) was used in all experiments. The fungus was stored at -80 ℃ as microconidial suspension with 30% glycerol. It was grown on potato dextrose agar (PDA) at 25 ℃ for 7 days in the dark to generate conidia. Spores were harvested using sterilized H_2O and filtrated through four layers of sterile lens paper. Cultures were inoculated at a concentration of 1×10^7 conidia/mL in YPD medium (2% peptone, 1% yeast extract, and 2% glucose) at 25 ℃ with shaking at 150 rpm. For conidial germination assay, fresh conidia of strains were harvested and adjusted to the concentration of 2.5 $\times10^5$ conidia/ml in PDB (liquid PDA). Twenty µl of the conidial suspension were dropped onto coverslips and incubated in a moist chamber with a temperature of 25 ℃. At least three independent experiments with triple replicates per experiment were performed.

Target gene deletion, complementation, and overexpression

The *FoSir5* gene deletion mutant was generated using the standard one-step gene replacement strategy (Figure 2-figure supplement 2A). First, 2 fragments with 0.7 kb of sequences flanking the targeted gene were PCR amplified with primer pairs UP-F/R and Down-F/R, respectively. Thereafter, the two flanking sequences were linked with a hygromycin-resistance cassette (HPH) by overlap PCR. The amplified fragment using primer pairs K-F/R was then purified and introduced into Fo protoplasts (Gronover, Kasulke et al., 2001, Jiang, Liu et al., 2011). Deletion mutants

were identified by PCR with primer pairs IN-F/R and OUT-F/R. For complementation, a fragment encompassing the entire *FoSir5* gene coding region and its native promoter region was amplified by PCR with primers FoSir5-C-F/R and inserted into pYF11 (G418 resistance) vector by the yeast gap repair approach (Bruno, Tenjo et al., 2004, Tang, Chen et al., 2020). Then, the construct was used for protoplast transformation of the ΔFoSir5 mutant.

For site-directed mutagenesis of *FoDLAT*, we first tried to delete the *FoDLAT* gene, however, despite numerous attempts (over 200 transformants), we failed to obtain knockout mutants, indicating that FoDLAT disruption was lethal in Fo. Alternatively, *FoDLAT*^{K148Q} or *FoDLAT*^{K148R} genes with native promoter region was generated by fusion PCR using primer FoDLAT-C-F/R and cloned into pYF11 plasmid to form GFP fusion constructs. Then the constructs were transformed into protoplast of Fo. After verification by PCR and sequencing, deletion of *FoDLAT* was performed as described above to generate strains FoDLAT^{K148Q} and FoDLAT^{K148R}, respectively.

For construction of the RP27:FoSir5/FoMDH/FoATP5H/FoCYC1:GFP vectors, we amplified fragments by PCR with primer pairs GFP-F/R of each gene, respectively. The fragments were then inserted into the pYF11 vector (Qi, Liu et al., 2016). For construction of the RP27:FoSir5/FoDLAT:Flag vectors, fragments amplified with primers FoSir5-Flag-F/R or FoDLAT-Flag-F/R were inserted into pHZ126 vector (hygromycin resistance). The constructs were then used for protoplast transformation of Fo or other strains. The primers used in this study were listed in

Supplementary File 3.

Epifluorescence microscopy

F. oxysporum cells expressing FoSir5-GFP or FoDLAT-GFP fusion proteins were incubated on PDA plates at 25 ℃ for 3 days. The mycelia of the tested strains were then collected and preincubated for 15 min with 200 nM MitoTracker Red CMRos (M7512, Invitrogen). After washing with phosphate-buffered saline (PBS), pH 7.4, the mycelia were stained with 1 μg/mL DAPI (D9542, Sigma) at room temperature in darkness for 5 min, followed by washing with PBS 3 times. Fluorescence microscope was performed using microscope of EVOS™ M5000 (Invitrogen).

Subcellular fractionation analysis

The nuclear and cytosolic proteins were extracted using Nuclear Protein Extraction Kit (R0050, Solarbio) and mitochondrial proteins were extracted by Mitochondrial Extraction Kit (SM0020, Solarbio), according to the instructions of the manufacturer. The obtained proteins were separated by SDS-PAGE and immunoblotted using anti-GFP (ab290, Abcam), anti-H3 (ab1791, Abcam), anti-Tubulin (PTM-1011, PTM Biolabs), and anti-ATP5A1 (459240, Thermo Fisher).

***In vitro* HDCR assays**

pET28 construct containing His fused FoSir5 was expressed in BL21 *Escherichia coli*. Protein expression was induced by adding isopropyl β-D-1-thiogalactopyranoside

(IPTG) to a final concentration of 0.2 mM when OD600 reached 0.6, and the culture was further grown at 16 ℃ overnight. Cells were harvested and resuspended in lysis buffer A (50 mM Tris-HCl, pH 7.5, 300 mM NaCl, 1 mM PMSF, and Roche EDTA free protease inhibitor). Following sonication and centrifugation, the supernatant was loaded onto a nickel column pre-equilibrated with lysis buffer. The column was washed with 5 column volumes of wash buffer (lysis buffer with 20 mM imidazole) and the bound proteins were then eluted with elution buffer (lysis buffer with 200 mM imidazole). After purification, proteins were dialyzed at 4 ℃ overnight. *In vitro* enzymatic reactions were performed as described previously (Liu et al., 2017). In brief, 50 μg native calf thymus histones (CTH, A002544, Sangon Biotech) were incubated with 0.5 μg recombinant FoSir5 protein at 30 ℃ for 1 hr in HDCR buffer (50 mM Tris pH 7.5, 5% glycerol, 5 mM NAD^+, 0.1 mM EDTA, 50 mM NaCl, and 0.2 mM PMSF) in the presence of 50, 100, or 200 μM crotonyl-CoA (C4282, Sigma). The assay mixture was then analyzed using western blotting by anti-PanKcr (PTM-501, PTM Biolabs) and anti-H3 (ab1791, Abcam).

Immunoprecipitation and mass spectrometry

For identification of FoSir5 interacting proteins, mycelium of Fo and FoSir5-GFP strains were collected and frozen with liquid nitrogen. For total protein extraction, the samples were ground into a fine powder in liquid nitrogen and resuspended in lysis buffer (10 mM Tris-HCl, pH 7.5, 150 mM NaCl, 0.5 mM EDTA, 0.5% NP-40) with 2 mM PMSF and proteinase inhibitor cocktail (Roche). The supernatant lysates were

then incubated with anti-GFP agarose (KTSM1301, KT HEALTH) at 4 ℃ for 2 h with gently shaking. Proteins bound to the beads were eluted after a serious of washing steps by PBS. Elution buffer (200 mM glycine, pH 2.5) and neutralization buffer (1 M Tris base, pH 10.4) were used for the elution process. For identification of crotonylation sites of FoDLAT, total proteins were isolated from FoDLAT-GFP strain and incubated with anti-GFP agarose. The eluted mixture was subsequently analyzed using liquid chromatography-tandem mass spectrometry (LC-MS/MS) conducted in PTM BIOLABS (Hangzhou, China).

Protein pull-down assays

Coding domain sequence of FoDLAT or FoDLAT^{K148Q} was cloned in pMAL vector for the N-terminal fusion with MBP. The fusion proteins were expressed in BL21 *E. coli*. Transformed cells were induced by adding IPTG to a final concentration of 0.2 mM when OD600 reached 0.6, and the culture was further grown at 37 ℃ for 3 hr. Cells were harvested by centrifugation and lysed by sonication in lysis buffer A. For purification, amylose resin (New England Biolabs) was added to the clarified lysate and incubated for 2 h at 4 ℃. Beads were then washed with 5 column volumes of PBS. MBP fusion proteins were eventually eluted in elution buffer supplemented with 20 mM maltose and then dialyzed at 4 ℃ overnight. For pull-down assay, 1 μg purified FoSir5-His protein was mixed with 1 μg MBP or MBP-FoDLAT protein in the binding buffer (50 mM HEPES, pH 7.5, 1 mM EDTA, 150 mM NaCl, 0.5 mM DTT, and 0.8% glycerol) in a total volume of 100 μl at room temperature for 1 h. 30

573 µl of amylose resin was added into the mixture and rotated at room temperature for 1
574 h. The mixture was subsequently washed three times with 1 mL of binding buffer, and
575 washed beads were boiled in 30 µl of 2 × SDS sampling buffer at 100 ℃ for 5 min.
576 The assay mixture was then analyzed using western blotting by anti-MBP (New
577 England Biolabs) and anti-His (D2951, Beyotime).
578

579 **Generation of anti-K148cr-FoDLAT antibody**

580 FoDLAT K148 site-specific crotonylation antibody was generated by using a
581 FoDLAT crotonylated peptide (KEEKSESK(cr)SESASAC) conjugated to KLH as an
582 antigen. Antibodies were produced from rabbits by HUABIO (Hangzhou, China). The
583 specificity of the antibody was tested by immunoblot analysis.
584

585 ***In vivo* decrotonylation assay**

586 For construction of the RP27:FoDLAT/FoDLAT^{K148Q} /FoDLAT^{K148R}:GFP vectors, we
587 amplified fragments by PCR with primers FoDLAT-GFP-F/R, respectively. The
588 fragments were then inserted into the pYF11 vector. Afterwards, the constructs were
589 transformed into Fo, ΔFoSir5, and OE-1, respectively. GFP fusion proteins in different
590 pairs of strains were immunoprecipitated as described above. The eluted proteins were
591 then analyzed by western blot using anti-GFP, anti-Kcr (PTM-501, PTM Biolabs),
592 anti-Ksu (PTM-419, PTM Biolabs), anti-Kma (PTM-902, PTM Biolabs) and
593 anti-Kglu (PTM-1152, PTM Biolabs), followed by quantification using Quantity One
594 (Bio-Rad).

595

596 ***In vitro* decrotonylation assay**

597 Fifty ng of MBP-FoDLAT protein (WT or K148Q) was incubated with or without 50
598 ng FoSir5-His protein in the absence or presence of 5 mM NAD^+ in 200 μl HDCR
599 buffer for 1 h at 30 ℃. Samples were analyzed by western blot using anti-PanKcr and
600 anti-MBP, followed by quantification using Quantity One (Bio-Rad).

601

602 **PDC enzyme assay**

603 PDC activity was measured according to the protocol by PDC activity assay kit
604 (ab109902, Abcam). The germinating conidia of the tested strains were grown in YPD
605 at 25 ℃ for 8 h in a shaker. The total extracts were diluted and added into the
606 microplate. After incubation in the plate for 3 hours at room temperature, the samples
607 were stabilized and incubated with assay buffer. The fluorescence was measured at
608 450 nm for 20 minutes with 20 seconds interval among each measurement, and the
609 slope of the line indicated the PDC activity. The rates were determined as change in
610 OD over time, represented as change in milliOD per minute.

611

612 **Quantification of acetyl-CoA**

613 Acetyl-coA was measured using an acetyl-CoA assay kit (BC0980, Solarbio). The
614 germinating conidia of the tested strains grown in YPD at 25 ℃ for 8 h in a shaker
615 were harvested and homogenized in lysis buffer of the kit in ice. The supernatant was
616 used to determine acetyl-CoA concentration in triplicate according to manufacturer's

617 instructions.

618

619 **Quantification of ATP**

620 The ATP assay kit (S0026, Beyotime), which employs the luciferin-luciferase method
621 (Drew & Leeuwenburgh, 2003), was used to quantify ATP. The working solution was
622 prepared according to the kit protocol. The germinating conidia of the tested strains
623 grown in YPD at 25 ℃ for 8 h in a shaker were harvested and homogenized in lysis
624 buffer. Then, 100 μl of working solution and 20 μl of supernatant of the total extracts
625 were added to each well of a 96-well microtiter plate. The luciferase signals was
626 detected by a multifunctional microplate reader (SpectraMax M2) for 30 s. The
627 standard curve of ATP concentration from 1 pM to 1 μM was prepared by gradient
628 dilution.

629

630 **RNA sequencing**

631 The germinating conidia of Fo and ΔFoSir5 with three biological replicates were
632 harvested after growth in YPD medium with shaking at 150 rpm for 8 h in 25 ℃.
633 Total RNA was extracted using the TRIzol reagent according to the instructions of
634 manufacturer. RNA-seq data were analyzed as previously described (Rodenburg,
635 Terhem et al., 2018). Briefly, Cutadapt (v1.16) software was used to filter the
636 sequencing data. Reference genome index was built by Bowtie2 (2.2.6) and the
637 filtered reads were mapped to the reference genome using Tophat2 (2.0.14). HTSeq
638 (0.9.1) statistics was used to compare the Read Count values on each gene as the

original expression of the gene, and then FPKM was used to standardize the expression. DESeq (1.30.0) was used to analyze the genes of difference expression with screened conditions as follows: an absolute $\log_2$ value > 1 and P value < 0.05. All the detected genes were shown in Supplementary File 2.

Fluorescent Real-time qPCR

For qRT-PCR assessment of *FoSir5* expression, fresh spores were inoculated in YPD medium at 25 ℃ with shaking at 150 rpm. At 0, 4, 8, 12 and 24 h, the cultures were centrifuged at 12,000×g for 15 min and the pellets were collected for RNA extraction. For validation of RNA-seq data, three batches of biological repeats of Fo and ΔFoSir5 were independently collected. RNA was extracted and reverse transcribed using All-In-One RT MasterMix (abm). qRT-PCR was performed using M5 HiPer SYBR Premix EsTaq (Mei5bio). The transcript abundance of candidate genes were calculated using the $2^{-\triangle Ct}$ method, normalized to *FoEF-1α* (Elongation factor 1α). All primers used for qRT-qPCR were listed in Supplementary File 3.

ChIP-qPCR analysis

ChIP was performed according to described methods (Liu, Jian et al., 2019). Briefly, the germinating conidia of different strains were harvested after growth in YPD medium with shaking at 150 rpm for 8 h in 25 ℃. The germinating conidia were cross-linked with 1% formaldehyde gently shaking for 25 min and then stopped with glycine with a final concentration of 125 mM for another incubation of 10 min. After

cleaning with sterile water for several times, the cultures were frozen and ground with liquid nitrogen. The powder was re-suspended in the lysis buffer (250 mM HEPES pH 7.5, 1 mM EDTA, 150 mM NaCl, 10 mM DTT, 0.1% deoxycholate, and 1% Triton) and protease inhibitor cocktail (Roche) with a conidia/buffer ratio as 0.2g/2ml. The DNA was sheared into ~500 bp fragments using sonicator (Bioruptor Plus CHIP, ultrasonication for 30s and stop for 30s, 10 times). The supernatant was diluted after centrifugation with ChIP dilution buffer (1.1% Triton X-100, 16.7 mM Tris-HCl pH 8.0, 1.2 mM EDTA, 167 mM NaCl). Immunoprecipitation was conducted using 5 µl anti-GFP antibody (ab290, Abcam) or 5 µl anti-H3K18cr antibody (PTM-517, PTM Biolabs) together with protein A agarose (Roche) overnight at 4 ℃. After separation, beads were washed orderly by low-salt wash buffer (150 mM NaCl, 0.2% SDS, 20 mM Tris-HCl pH 8.0, 2 mM EDTA, 0.5% TritonX-100), high salt wash buffer (500 mM NaCl, 2 mM EDTA, 20 mM Tris-HCl pH 8.0, 0.2% SDS, 0.5% Triton X-100), LiCl wash buffer (0.25 M LiCl, 1% Nonidet P-40, 1% sodium deoxycholate, 1 mM EDTA, 10 mM Tris-HCl pH 8.0), and TE buffer. DNA bound to the beads was then eluted and precipitated. ChIP-qPCR was independently repeated three times. Relative enrichment values were calculated by dividing the immunoprecipitated DNA by the input DNA and internal control gene (*β-tubulin*). Primers using for ChIP-qPCR were designed near putative TSS and listed in Supplementary File 3.

Infection assays of *F. oxysporum* on tomato seedlings

Briefly, 2-week-old tomato seedlings were used for root dip infection for 10 min in

683 spore suspension (10^6 spores/mL). The infected plants were transplanted in sterile
684 soil-vermiculite mixture (1:1 ratio) and kept in plant growth chamber at 25 ℃ and 90%
685 relative humidity (RH). Severity of disease symptoms was recorded and scored
686 according to the values ranging from 1 to 5: 1- few symptoms, only first true leaf
687 necrotic or curled; 2- clear symptoms, first three leaves developed symptoms; 3-
688 severe symptoms, leaves necrotic and curled, defoliation, growth retardation; 4- rotted
689 plant but still alive; 5- dead plant. Disease index was calculated using the following
690 formula: Disease index=Σ (number of leaves in each disease grade×grades
691 value)/(total number of assessed leaves×the highest grade value) (Yuan, Huang et al.,
692 2019). This inoculation experiment was repeated twice to verify consistency in the
693 observed results. qRT-PCR analysis of *F. oxysporum EF-1α* transcript levels was
694 performed using tomato plants harvested after 14-day infection with different strains.
695 The expression of tomato *RCE1*, a constitutively expressed gene, was used as a
696 control for the use of equal amounts of RNA for RT-PCR.
697
698
699
700
701
702
703
704

Acknowledgements

This research was supported by the National Natural Science Foundation of China (31972213 and 32102149), the Shandong Provincial Natural Science Foundation (ZR2019BC070 and ZR2020KC003), Shandong Province "Double-Hundred Talent Plan" (WST2018008), and Taishan Scholar Construction Foundation of Shandong Province (tshw20130963). X.P. and B.F.L. were supported by the Wellcome Trust (200873/Z/16/Z).

Data availability

The RNA-seq raw reads are available in NCBI Sequence Read Archive (SRA) database with the accession number of PRJNA687117.

Competing interests

The authors declare that no competing interests exist.

References

Bao X, Wang Y, Li X, Li X-M, Liu Z, Yang T, Wong CF, Zhang J, Hao Q, Li XD (2014) Identification of 'erasers' for lysine crotonylated histone marks using a chemical proteomics approach. *Elife* 3: e02999

Bell EL, Guarente L (2011) The SirT3 divining rod points to oxidative stress. *Molecular Cell* 42: 561-568

Boivin A, Gaumer S, Sainsard-Chanet A (2008) Life span extension by dietary restriction is reduced but not abolished by loss of both SIR2 and HST2 in Podospora anserina. *Mechanisms of ageing and development* 129: 714-21

Bruno KS, Tenjo F, Li L, Hamer JE, Xu JR (2004) Cellular localization and role of kinase activity of PMK1 in Magnaporthe grisea. *Eukaryotic cell* 3: 1525-32

Byles V, Chmilewski LK, Wang J, Zhu L, Forman LW, Faller DV, Dai Y (2010) Aberrant cytoplasm localization and protein stability of SIRT1 is regulated by PI3K/IGF-1R signaling in human cancer cells. *International journal of biological sciences* 6: 599-612

Cen Y, Y Youn D, A Sauve A (2011) Advances in characterization of human sirtuin isoforms: chemistries, targets and therapeutic applications. *Current medicinal chemistry* 18: 1919-1935

Chen Y, Sprung R, Tang Y, Ball H, Sangras B, Kim SC, Falck JR, Peng J, Gu W, Zhao Y (2007) Lysine propionylation and butyrylation are novel post-translational modifications in histones. *Molecular & Cellular Proteomics* 6: 812-819

Deng GM, Yang QS, He WD, Li CY, Yang J, Zuo CW, Gao J, Sheng O, Lu SY, Zhang S, Yi GJ (2015) Proteomic analysis of conidia germination in Fusarium oxysporum f. sp. cubense tropical race 4 reveals new targets in ergosterol biosynthesis pathway for controlling Fusarium wilt of banana. *Applied microbiology and biotechnology* 99: 7189-207

Drew B, Leeuwenburgh C (2003) Method for measuring ATP production in isolated mitochondria: ATP production in brain and liver mitochondria of Fischer-344 rats with age and caloric restriction. *American journal of physiology Regulatory, integrative and comparative physiology* 285: R1259-67

Du J, Zhou Y, Su X, Yu JJ, Khan S, Jiang H, Kim J, Woo J, Kim JH, Choi BH, He B, Chen W, Zhang S, Cerione RA, Auwerx J, Hao Q, Lin H (2011) Sirt5 is a NAD-dependent protein lysine demalonylase and desuccinylase. *Science* 334: 806-9

Dubey A, Lee J, Kwon S, Lee YH, Jeon J (2019) A MYST family histone acetyltransferase, MoSAS3, is required for development and pathogenicity in the rice blast fungus. *Mol Plant Pathol* 20: 1491-1505

Feldman JL, Baeza J, Denu JM (2013) Activation of the protein deacetylase SIRT6 by long-chain fatty acids and widespread deacylation by mammalian sirtuins. *Journal of Biological Chemistry* 288: 31350-31356

Fernandez J, Marroquin-Guzman M, Nandakumar R, Shijo S, Cornwell KM, Li G, Wilson RA (2014) Plant defence suppression is mediated by a fungal sirtuin during rice infection by Magnaporthe oryzae. *Mol Microbiol* 94: 70-88

Gertz M, Steegborn C (2016) Using mitochondrial sirtuins as drug targets: disease implications and available compounds. *Cellular and molecular life sciences : CMLS* 73: 2871-96

Gronover CS, Kasulke D, Tudzynski P, Tudzynski B (2001) The role of G protein alpha subunits in the infection process of the gray mold fungus Botrytis cinerea. *Mol Plant Microbe Interact* 14:

1293-302

Haigis MC, Sinclair DA (2010) Mammalian sirtuins: biological insights and disease relevance. *Annual review of pathology* 5: 253-95

Hirschey MD, Zhao Y (2015) Metabolic Regulation by Lysine Malonylation, Succinylation, and Glutarylation. *Molecular & cellular proteomics : MCP* 14: 2308-15

Itoh E, Shigemoto R, Oinuma KI, Shimizu M, Masuo S, Takaya N (2017) Sirtuin A regulates secondary metabolite production by Aspergillus nidulans. *J Gen Appl Microbiol* 63: 228-235

Jiang J, Liu X, Yin Y, Ma Z (2011) Involvement of a velvet protein FgVeA in the regulation of asexual development, lipid and secondary metabolisms and virulence in Fusarium graminearum. *Plos One* 6: e28291

Kanfi Y, Naiman S, Amir G, Peshti V, Zinman G, Nahum L, Bar-Joseph Z, Cohen HY (2012) The sirtuin SIRT6 regulates lifespan in male mice. *Nature* 483: 218-221

Kawauchi M, Nishiura M, Iwashita K (2013) Fungus-specific sirtuin HstD coordinates secondary metabolism and development through control of LaeA. *Eukaryotic cell* 12: 1087-96

Kim SC, Sprung R, Chen Y, Xu Y, Ball H, Pei J, Cheng T, Kho Y, Xiao H, Xiao L, Grishin NV, White M, Yang XJ, Zhao Y (2006) Substrate and functional diversity of lysine acetylation revealed by a proteomics survey. *Mol Cell* 23: 607-18

Kwon OK, Kim SJ, Lee S (2018) First profiling of lysine crotonylation of myofilament proteins and ribosomal proteins in zebrafish embryos. *Sci Rep* 8: 3652

Leroch M, Kleber A, Silva E, Coenen T, Koppenhöfer D, Shmaryahu A, Valenzuela PD, Hahn M (2013) Transcriptome profiling of Botrytis cinerea conidial germination reveals upregulation of infection-related genes during the prepenetration stage. *Eukaryotic cell* 12: 614-26

Li Y, Sabari BR, Panchenko T, Wen H, Zhao D, Guan H, Wan L, Huang H, Tang Z, Zhao Y, Roeder RG, Shi X, Allis CD, Li H (2016) Molecular Coupling of Histone Crotonylation and Active Transcription by AF9 YEATS Domain. *Mol Cell* 62: 181-193

Liu S, Xue C, Fang Y, Chen G, Peng X, Zhou Y, Chen C, Liu G, Gu M, Wang K, Zhang W, Wu Y, Gong Z (2018) Global Involvement of Lysine Crotonylation in Protein Modification and Transcription Regulation in Rice. *Molecular & cellular proteomics : MCP* 17: 1922-1936

Liu S, Yu H, Liu Y, Liu X, Zhang Y, Bu C, Yuan S, Chen Z, Xie G, Li W (2017) Chromodomain protein CDYL acts as a crotonyl-CoA hydratase to regulate histone crotonylation and spermatogenesis. *Molecular Cell* 67: 853-866. e5

Liu Z, Jian Y, Chen Y, Kistler HC, He P, Ma Z, Yin Y (2019) A phosphorylated transcription factor regulates sterol biosynthesis in Fusarium graminearum. *Nat Commun* 10: 1228

Lombard DB, Alt FW, Cheng HL, Bunkenborg J, Streeper RS, Mostoslavsky R, Kim J, Yancopoulos G, Valenzuela D, Murphy A, Yang Y, Chen Y, Hirschey MD, Bronson RT, Haigis M, Guarente LP, Farese RV, Jr., Weissman S, Verdin E, Schwer B (2007) Mammalian Sir2 homolog SIRT3 regulates global mitochondrial lysine acetylation. *Mol Cell Biol* 27: 8807-14

Mathias RA, Greco TM, Oberstein A, Budayeva HG, Chakrabarti R, Rowland EA, Kang Y, Shenk T, Cristea IM (2014) Sirtuin 4 is a lipoamidase regulating pyruvate dehydrogenase complex activity. *Cell* 159: 1615-25

Michielse CB, Rep M (2009) Pathogen profile update: Fusarium oxysporum. *Molecular Plant Pathology* 10: 311-324

Michishita E, Park JY, Burneskis JM, Barrett JC, Horikawa I (2005) Evolutionarily conserved and nonconserved cellular localizations and functions of human SIRT proteins. *Molecular biology of*

the cell 16: 4623-35

North BJ, Verdin E (2004) Sirtuins: Sir2-related NAD-dependent protein deacetylases. *Genome biology* 5: 224

Nucci M, Anaissie E (2007) Fusarium infections in immunocompromised patients. *Clinical microbiology reviews* 20: 695-704

Park J, Chen Y, Tishkoff DX, Peng C, Tan M, Dai L, Xie Z, Zhang Y, Zwaans BM, Skinner ME, Lombard DB, Zhao Y (2013) SIRT5-mediated lysine desuccinylation impacts diverse metabolic pathways. *Mol Cell* 50: 919-30

Qi Z, Liu M, Dong Y, Zhu Q, Li L, Li B, Yang J, Li Y, Ru Y, Zhang H, Zheng X, Wang P, Zhang Z (2016) The syntaxin protein (MoSyn8) mediates intracellular trafficking to regulate conidiogenesis and pathogenicity of rice blast fungus. *The New phytologist* 209: 1655-67

Rardin MJ, He W, Nishida Y, Newman JC, Carrico C, Danielson SR, Guo A, Gut P, Sahu AK, Li B (2013) SIRT5 regulates the mitochondrial lysine succinylome and metabolic networks. *Cell metabolism* 18: 920-933

Rodenburg SYA, Terhem RB, Veloso J, Stassen JHM, van Kan JAL (2018) Functional Analysis of Mating Type Genes and Transcriptome Analysis during Fruiting Body Development of Botrytis cinerea. *MBio* 9

Ryan MT (2018) Mitochondria - The energy powerhouses. *Semin Cell Dev Biol* 76: 130-131

Sabari BR, Tang Z, Huang H, Yong-Gonzalez V, Molina H, Kong HE, Dai L, Shimada M, Cross JR, Zhao Y, Roeder RG, Allis CD (2015) Intracellular crotonyl-CoA stimulates transcription through p300-catalyzed histone crotonylation. *Mol Cell* 58: 203-15

Sharma M, Sengupta A, Ghosh R, Agarwal G, Tarafdar A, Nagavardhini A, Pande S, Varshney RK (2016) Genome wide transcriptome profiling of Fusarium oxysporum f sp. ciceris conidial germination reveals new insights into infection-related genes. *Sci Rep* 6: 37353

Smith KM, Kothe GO, Matsen CB, Khlafallah TK, Adhvaryu KK, Hemphill M, Freitag M, Motamedi MR, Selker EU (2008) The fungus Neurospora crassa displays telomeric silencing mediated by multiple sirtuins and by methylation of histone H3 lysine 9. *Epigenetics & chromatin* 1: 5

Sun CF, Xu WF, Zhao QW, Luo S, Chen XA, Li YQ, Mao XM (2020) Crotonylation of key metabolic enzymes regulates carbon catabolite repression in Streptomyces roseosporus. *Communications biology* 3: 192

Sun H, Liu X, Li F, Li W, Zhang J, Xiao Z, Shen L, Li Y, Wang F, Yang J (2017) First comprehensive proteome analysis of lysine crotonylation in seedling leaves of Nicotiana tabacum. *Sci Rep* 7: 3013

Sun J, Qiu C, Qian W, Wang Y, Sun L, Li Y, Ding Z (2019) Ammonium triggered the response mechanism of lysine crotonylome in tea plants. *BMC genomics* 20: 340

Tan M, Luo H, Lee S, Jin F, Yang JS, Montellier E, Buchou T, Cheng Z, Rousseaux S, Rajagopal N (2011a) Identification of 67 histone marks and histone lysine crotonylation as a new type of histone modification. *Cell* 146: 1016-1028

Tan M, Luo H, Lee S, Jin F, Yang JS, Montellier E, Buchou T, Cheng Z, Rousseaux S, Rajagopal N, Lu Z, Ye Z, Zhu Q, Wysocka J, Ye Y, Khochbin S, Ren B, Zhao Y (2011b) Identification of 67 histone marks and histone lysine crotonylation as a new type of histone modification. *Cell* 146: 1016-28

Tan M, Peng C, Anderson KA, Chhoy P, Xie Z, Dai L, Park J, Chen Y, Huang H, Zhang Y (2014a) Lysine glutarylation is a protein posttranslational modification regulated by SIRT5. *Cell metabolism* 19: 605-617

Tan M, Peng C, Anderson KA, Chhoy P, Xie Z, Dai L, Park J, Chen Y, Huang H, Zhang Y, Ro J,

Wagner GR, Green MF, Madsen AS, Schmiesing J, Peterson BS, Xu G, Ilkayeva OR, Muehlbauer MJ, Braulke T et al. (2014b) Lysine glutarylation is a protein posttranslational modification regulated by SIRT5. *Cell Metab* 19: 605-17

Tang G, Chen A, Dawood DH, Liang J, Chen Y, Ma Z (2020) Capping proteins regulate fungal development, DON-toxisome formation and virulence in Fusarium graminearum. *Mol Plant Pathol* 21: 173-187

Vaquero A, Scher MB, Lee DH, Sutton A, Cheng HL, Alt FW, Serrano L, Sternglanz R, Reinberg D (2006) SirT2 is a histone deacetylase with preference for histone H4 Lys 16 during mitosis. *Genes Dev* 20: 1256-61

Wan J, Liu H, Chu J, Zhang H (2019) Functions and mechanisms of lysine crotonylation. *Journal of cellular and molecular medicine* 23: 7163-7169

Wang J, Mei H, Zheng C, Qian H, Cui C, Fu Y, Su J, Liu Z, Yu Z, He J (2013) The metabolic regulation of sporulation and parasporal crystal formation in Bacillus thuringiensis revealed by transcriptomics and proteomics. *Molecular & cellular proteomics : MCP* 12: 1363-76

Wang JJ, Cai Q, Qiu L, Ying SH, Feng MG (2018) The histone acetyltransferase Mst2 sustains the biological control potential of a fungal insect pathogen through transcriptional regulation. *Applied microbiology and biotechnology* 102: 1343-1355

Wei W, Liu X, Chen J, Gao S, Lu L, Zhang H, Ding G, Wang Z, Chen Z, Shi T (2017a) Class I histone deacetylases are major histone decrotonylases: evidence for critical and broad function of histone crotonylation in transcription. *Cell research* 27: 898-915

Wei W, Mao A, Tang B, Zeng Q, Gao S, Liu X, Lu L, Li W, Du JX, Li J (2017b) Large-scale identification of protein crotonylation reveals its role in multiple cellular functions. *Journal of proteome research* 16: 1743-1752

Wu Q, Li W, Wang C, Fan P, Cao L, Wu Z, Wang F (2017) Ultradeep lysine Crotonylome reveals the Crotonylation enhancement on both histones and nonhistone proteins by SAHA treatment. *Journal of proteome research* 16: 3664-3671

Xiong X, Panchenko T, Yang S, Zhao S, Yan P, Zhang W, Xie W, Li Y, Zhao Y, Allis CD, Li H (2016) Selective recognition of histone crotonylation by double PHD fingers of MOZ and DPF2. *Nat Chem Biol* 12: 1111-1118

Xu W, Wan J, Zhan J, Li X, He H, Shi Z, Zhang H (2017) Global profiling of crotonylation on non-histone proteins. *Cell research* 27: 946-949

Yu H, Bu C, Liu Y, Gong T, Liu X, Liu S, Peng X, Zhang W, Peng Y, Yang J, He L, Zhang Y, Yi X, Yang X, Sun L, Shang Y, Cheng Z, Liang J (2020) Global crotonylome reveals CDYL-regulated RPA1 crotonylation in homologous recombination-mediated DNA repair. *Science advances* 6: eaay4697

Yuan M, Huang Y, Ge W, Jia Z, Song S, Zhang L (2019) Involvement of jasmonic acid, ethylene and salicylic acid signaling pathways behind the systemic resistance induced by Trichoderma longibrachiatum H9 in cucumber. *BMC genomics* 20: 144

Zhang N, Yang Z, Liang W, Liu M (2020a) Global Proteomic Analysis of Lysine Crotonylation in the Plant Pathogen Botrytis cinerea. *Front Microbiol* 11: 564350

Zhang N, Yang Z, Zhang Z, Liang W (2020b) BcRPD3-Mediated Histone Deacetylation Is Involved in Growth and Pathogenicity of Botrytis cinerea. *Front Microbiol* 11: 1832

Zhao D, Guan H, Zhao S, Mi W, Wen H, Li Y, Zhao Y, Allis CD, Shi X, Li H (2016) YEATS2 is a selective histone crotonylation reader. *Cell Res* 26: 629-32

Figure legends:

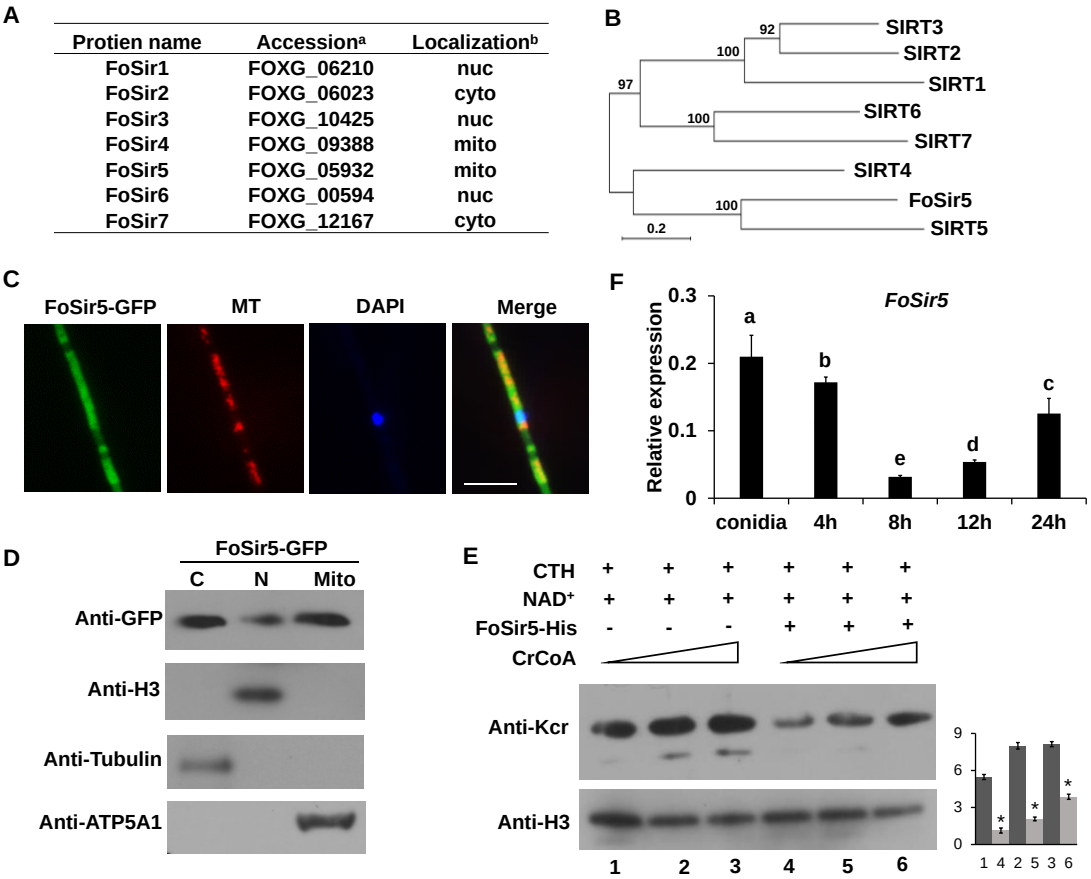

Figure 1. Cellular localization and activity of FoSir5 in *F. oxysporum*. **(A)** Sirtuin proteins in *F. oxysporum* with predicted subcellular localizations. [a] Accession number of the full-length protein sequence available at Ensembl. [b] Localization of the *F. oxysporum* Sir2 protein determined by WoLF PSORT. **(B)** Phylogenetic tree relating FoSir5 to the orthologous human Sirtuin isoforms SIRT1 (NP_036370), SIRT2 (NP_085096), SIRT3 (NP_001357239), SIRT4 (NP_036372), SIRT5 (NP_001363737), SIRT6 (NP_057623), and SIRT7 (NP_057622). The tree is based on neighbour-joining analysis using MEGA-X. **(C)** Fluorescence microscopy analysis of FoSir5-GFP localization with MitoTracker Red (MT) and DAPI. Scale bars = 10 µm. **(D)** Subcellular fractionation of FoSir5-GFP transformants in *F. oxysporum*.

914 Nuclear, cytoplasmic, and mitochondrial proteins were separately extracted and
915 FoSir5-GFP were detected with anti-GFP antibody (Materials and Methods). The
916 fractionation controls were ATP5A1 (mitochondria), Tubulin (cytosol), and histone
917 H3 (nucleus). C, cytosol; N, nucleus; Mito, mitochondria. **(E)** *In vitro* Kcr assays with
918 50 μg of native CTH, 5 mM NAD^+ and 0.5 μg of FoSir5-His in the presence of 50,
919 100, or 200 μM crotonyl-CoA. Reaction materials were analyzed by Western blotting
920 with anti-Kcr or anti-H3 antibody. Each scale bar represents the mean ± SD for
921 triplicate experiments. *indicates a significant difference between different pairs of
922 samples ($P < 0.05$). **(F)** Expression profile of *FoSir5* in conidia, mycelium and during
923 the germination process. The expression levels were normalized to that of the *F.*
924 *oxysporum* elongation factor 1 alpha (EF-1α) gene. The presence of different letters
925 above the mean values of three replicates indicates a significant difference between
926 different samples ($P < 0.05$, ANOVA).
927
928
929
930
931
932

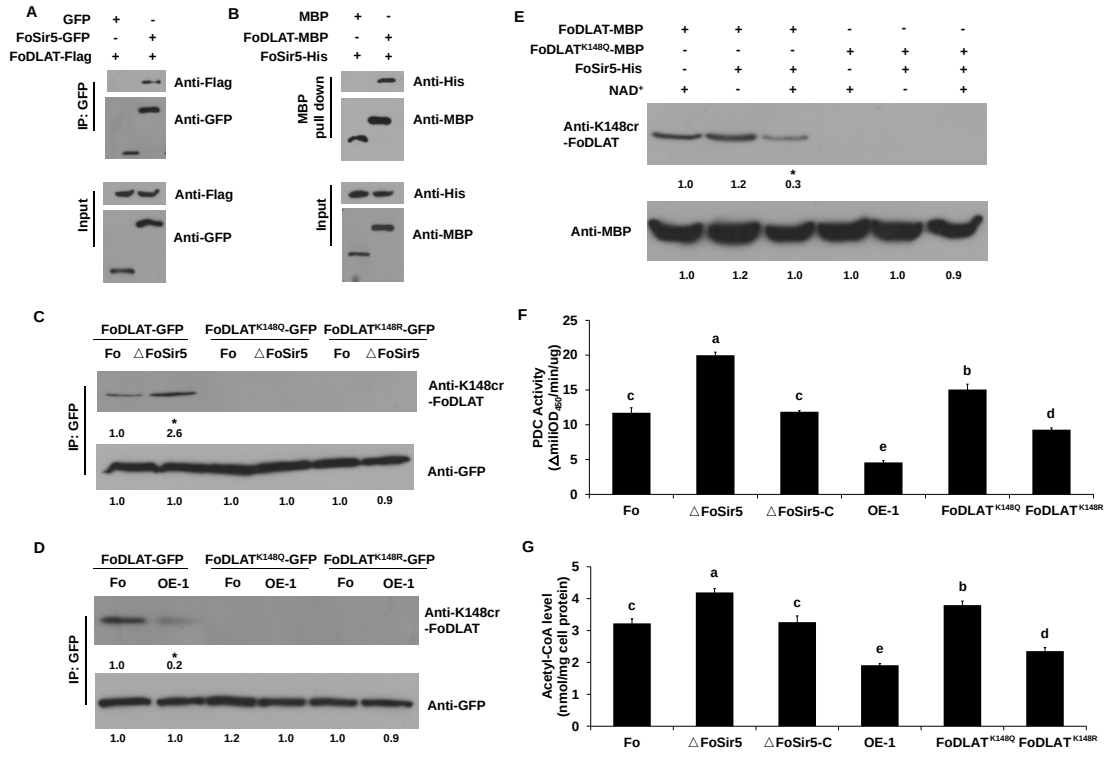

Figure 2. FoSir5 decrotonylates FoDLAT, the E2 component of *F. oxysporum* pyruvate decarboxylase complex, with regulatory consequence. **(A)** Co-IP assays reveal physical interaction of FoSir5-GFP and FoDLAT-Flag. Western blot analysis of cell extracts from transformants co-expressing FoDLAT-Flag with GFP or FoSir5-GFP and elution from anti-GFP agarose. The fusion proteins were detected with anti-Flag or anti-GFP antibody. **(B)** *In vitro* pull-down assays to detect FoSir5-His with MBP or the FoDLAT-MBP fusion protein. FoDLAT-MBP was used as bait to pull down the FoSir5-His protein from the induced cell extracts. The MBP protein was assayed as a negative control. Input and bound forms of the pull-down fractions were detected with anti-His or anti-MBP antibody. **(C-D)** The K148 crotonylation (anti-K148cr-FoDLAT, top panel) and amount (anti-GFP, bottom panel) of FoDLAT-GFP and its mutant isoforms in the ΔFoSir5 (C) and OE-1 strain (D).

946 Proteins were immunoprecipitated with anti-GFP antibody agarose beads and
947 analyzed by anti-K148cr-FoDLAT or anti-GFP antibody. Representative gels are
948 shown from experiments carried out at least twice. Numbers below the blots represent
949 the relative abundance of K148-crotonylated FoDLAT. Anti-GFP immunoblotting was
950 used to show equal loading. **(E)** FoSir5 directly decrotonylates FoDLAT *in vitro*.
951 Purified FoDLAT protein or its K148Q isoform (50 ng) were incubated with or
952 without 50 ng of purified FoSir5 in the absence or presence of 5 mM NAD^+ and then
953 analyzed by immunoblotting using anti-K148cr-FoDLAT or anti-His antibody. Each
954 gel shown is representative of two experiments. Numbers below the blots represent
955 the relative abundance of K148-crotonylated FoDLAT. Anti-MBP immunoblotting
956 was used to show equal loading. **(F-G)** FoSir5 and K148 mutant FoDLAT affected
957 PDC activity (F) and acetyl-CoA production (G) in *F. oxysporum*. PDC activity and
958 acetyl-CoA production were determined in germinating conidia at 8 h. The presence
959 of different letters above the mean values of three replicates indicates a significant
960 difference between different strains ($P < 0.05$, ANOVA).
961
962
963
964
965
966
967

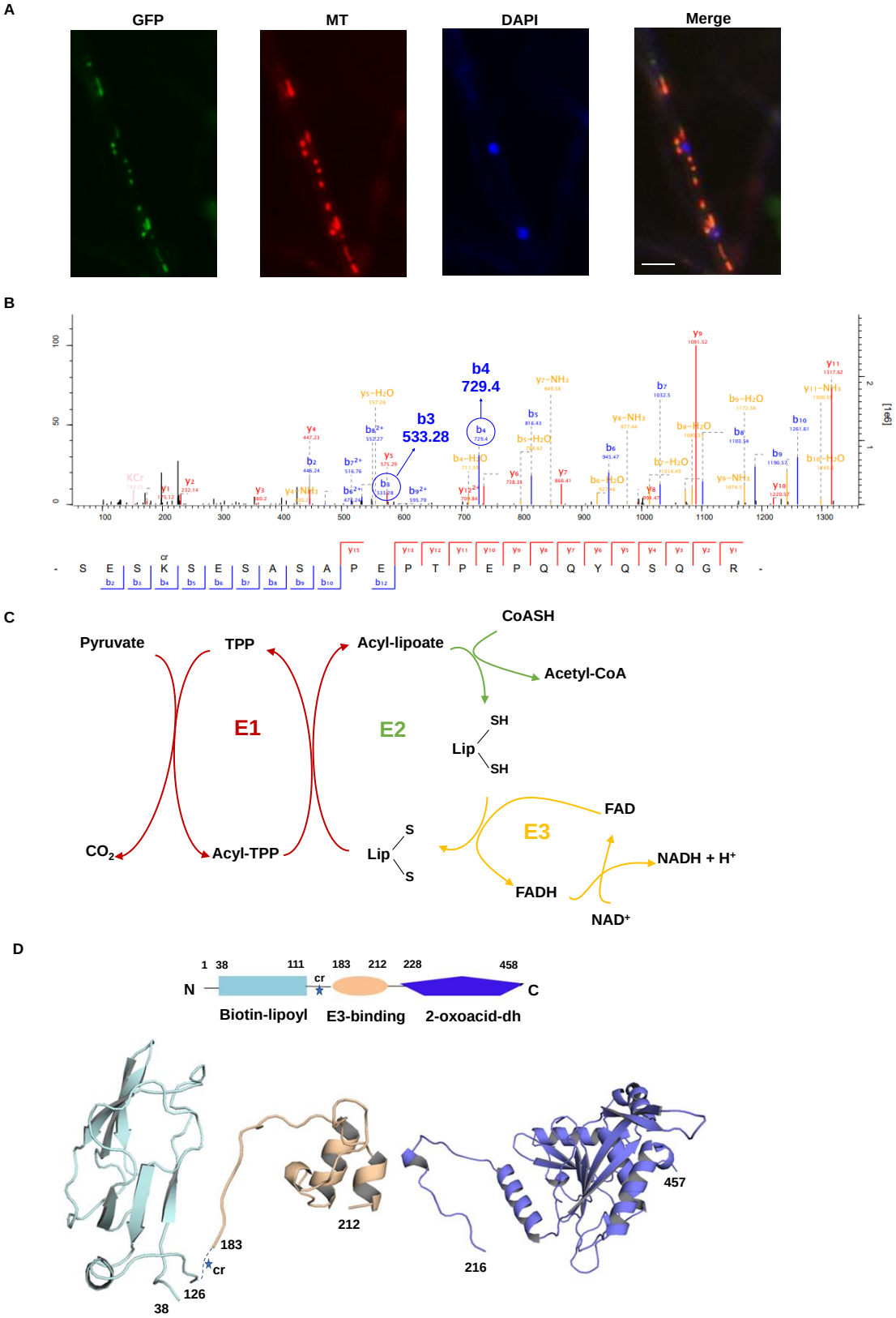

Figure 2-figure supplement 1. Interpretation of the subcellular location, Kcr site and protein structure of FoDLAT**. (A)** Fluorescence microscopy analysis of the

FoDLAT-GFP localization along with MitoTracker Red (MT) and DAPI. Scale bars = 10 µm. **(B)** Annotation of representative tandem mass spectra from trypsin-digested FoDLAT-GFP in *F. oxysporum* depicting K148 crotonylation. **(C)** Schematic of the chemical transformations catalysed by the E1 and E3 subunits of pyruvate dehydrogenase. **(D)** Homology models of the FoDLAT domains predicted by the PHYRE fold server. FoDALT domain boundary is defined using Motif program to against Pfam, NCBI-CDD database. The star indicates the K148 crotonylation site.

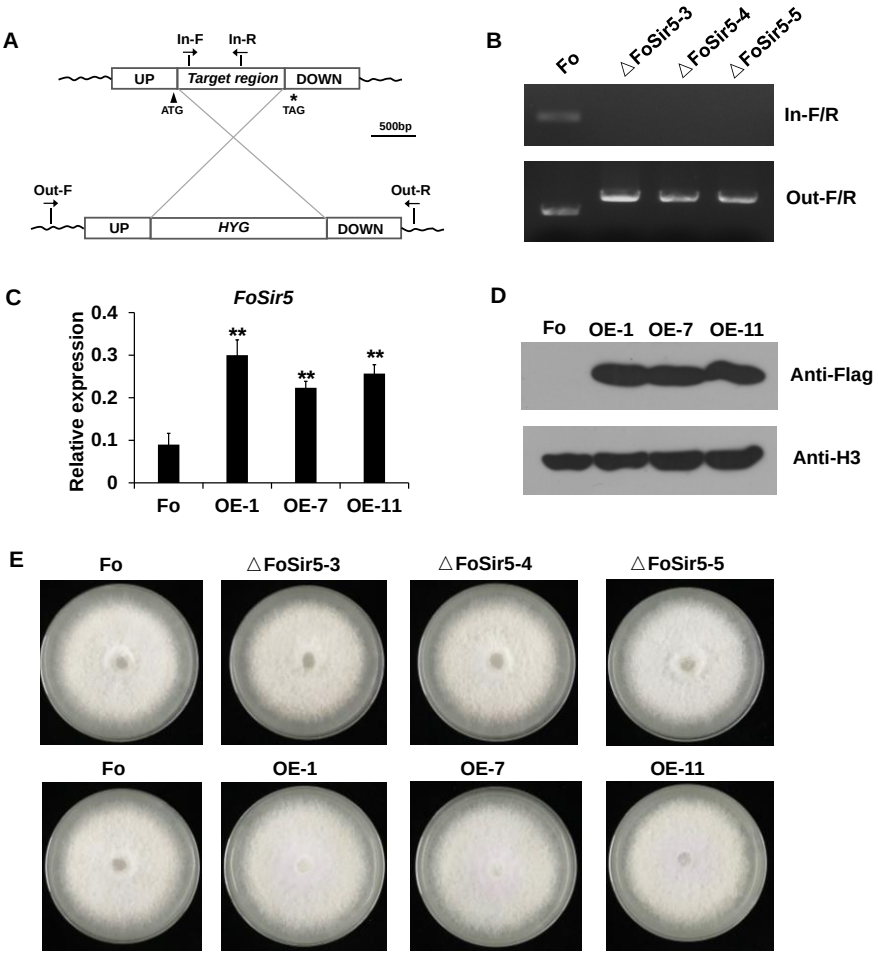

Figure 2-figure supplement 2. Generation of targeted *FoSir5* gene deletion mutants and overexpression transformants. **(A)** Schematic representation of the targeted deletion of *FoSir5*. **(B)** PCR analysis of targeted deletion in the ΔFoSir5 strains. Genomic DNA was analyzed by PCR with the primer pairs indicated in panel (A). **(C-D)** RT-PCR (C) and WB (D) analysis of the FoSir5-Flag-overexpression transformants. Data of RT-PCR are the means ± SDs (n = 3); **P < 0.05 by unpaired two-tailed t-test. **(E)** Mycelial growth of the indicated strains on PDA plates after 3 days of cultivation.

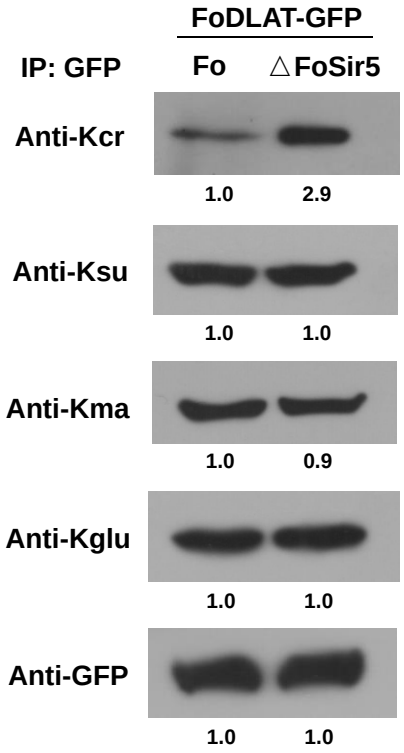

Figure 2-figure supplement 3. Detection of crotonylation, succinylation, malonylation, and glutarylation on FoDLAT protein in ΔFoSir5 compared with Fo. Proteins were immunoprecipitated with anti-GFP antibody agarose beads and analyzed by Western blot using the indicated antibodies. Representative gels are shown from experiments carried out at least twice. Anti-GFP immunoblotting was used to show equal loading.

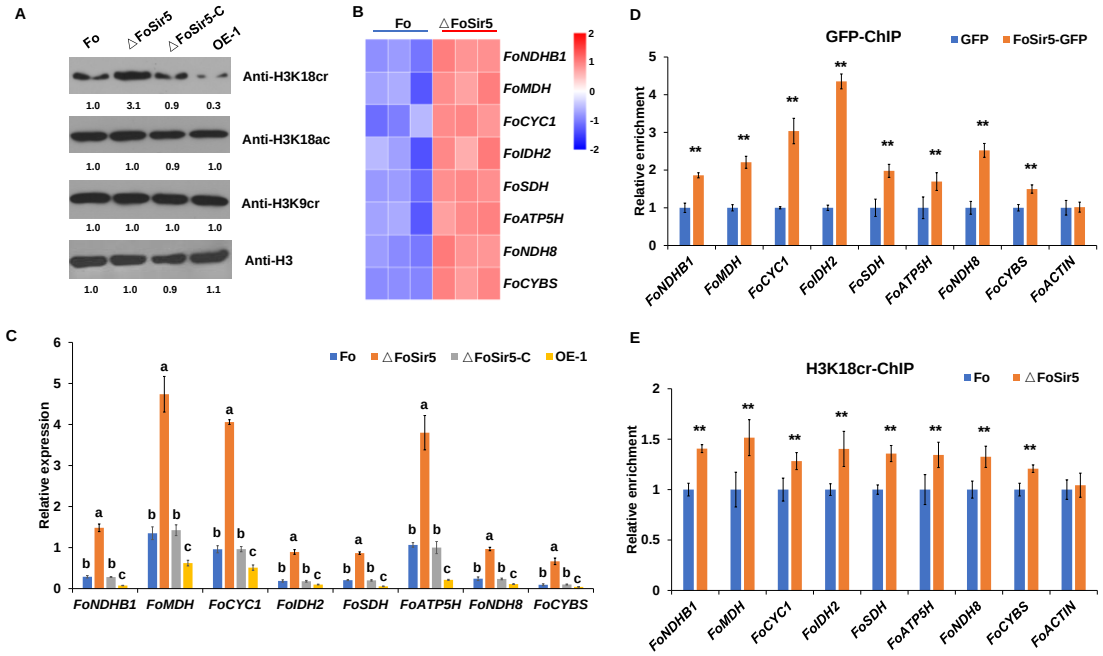

Figure 3. The downregulation of H3K18 crotonylation by FoSir5 and transcriptional repression of aerobic respiration-related genes. **(A)** Western blot analysis showed the effect of FoSir5 on histone H3K18 crotonylation and acetylation, and histone H3K9 crotonylation using the indicated antibodies. Numbers below the blots represent the relative abundance of different modifications. Anti-H3 immunoblotting was used to show equal loading. **(B)** RNA-seq analysis of 8 upregulated genes involved in aerobic respiration including *NDHB1* (NADH-quinone oxidoreductase chain B 1), *MDH* (malate dehydrogenase), *CYC1* (cytochrome C1), *IDH2* (isocitrate dehydrogenase subunit 2), *SDH* (succinate dehydrogenase), *ATP5H* (ATP synthase D chain), *NDH8* (NADH dehydrogenase iron-sulfur protein 8), and *CYBS* (succinate dehydrogenase cytochrome b small subunit). Differential expression in three biological replicates illustrated using a heat map with coloured squares indicating the range of expression referred to as the FPKM value. **(C)** qRT-PCR validation of

aerobic respiration-related genes in the indicated strains. The letters above the mean values of three replicates indicate significant differences between different strains ($P < 0.05$, ANOVA). **(D-E)** Relative enrichment of the immunoprecipitated promoter regions in aerobic respiration-related genes determined using anti-GFP antibody in the FoSir5-GFP strain and Fo strain containing GFP alone (D) or using anti-H3K18cr antibody in the Fo and ΔFoSir5 mutant strains (E). The fold enrichment was normalized to the input and internal control gene (*β-tubulin*). Data are the means ± SDs (n = 3); **$P < 0.05$ by unpaired two-tailed t-test.

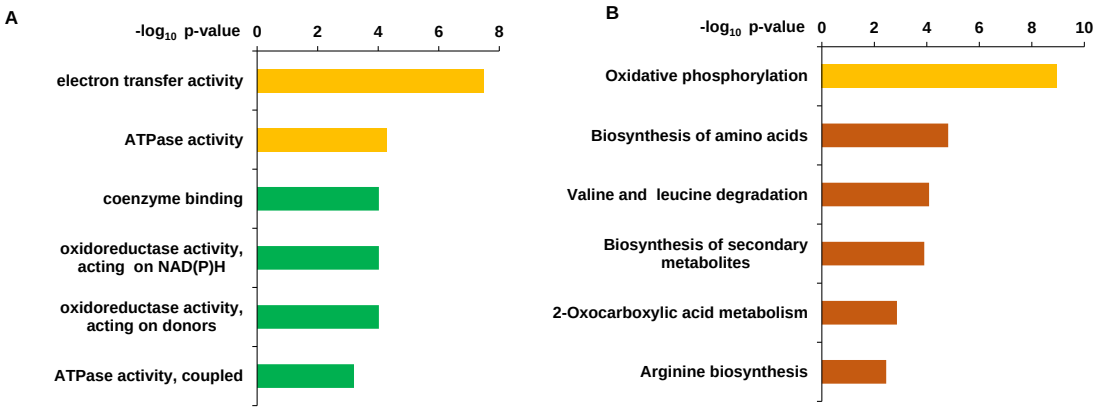

Figure 3-figure supplement 1. Distribution of functional classification of GO **(A)** and KEGG pathway **(B)** of the upregulated genes in ΔFoSir5 compared with Fo. Histograms indicate P-values of the enriched functional categories.

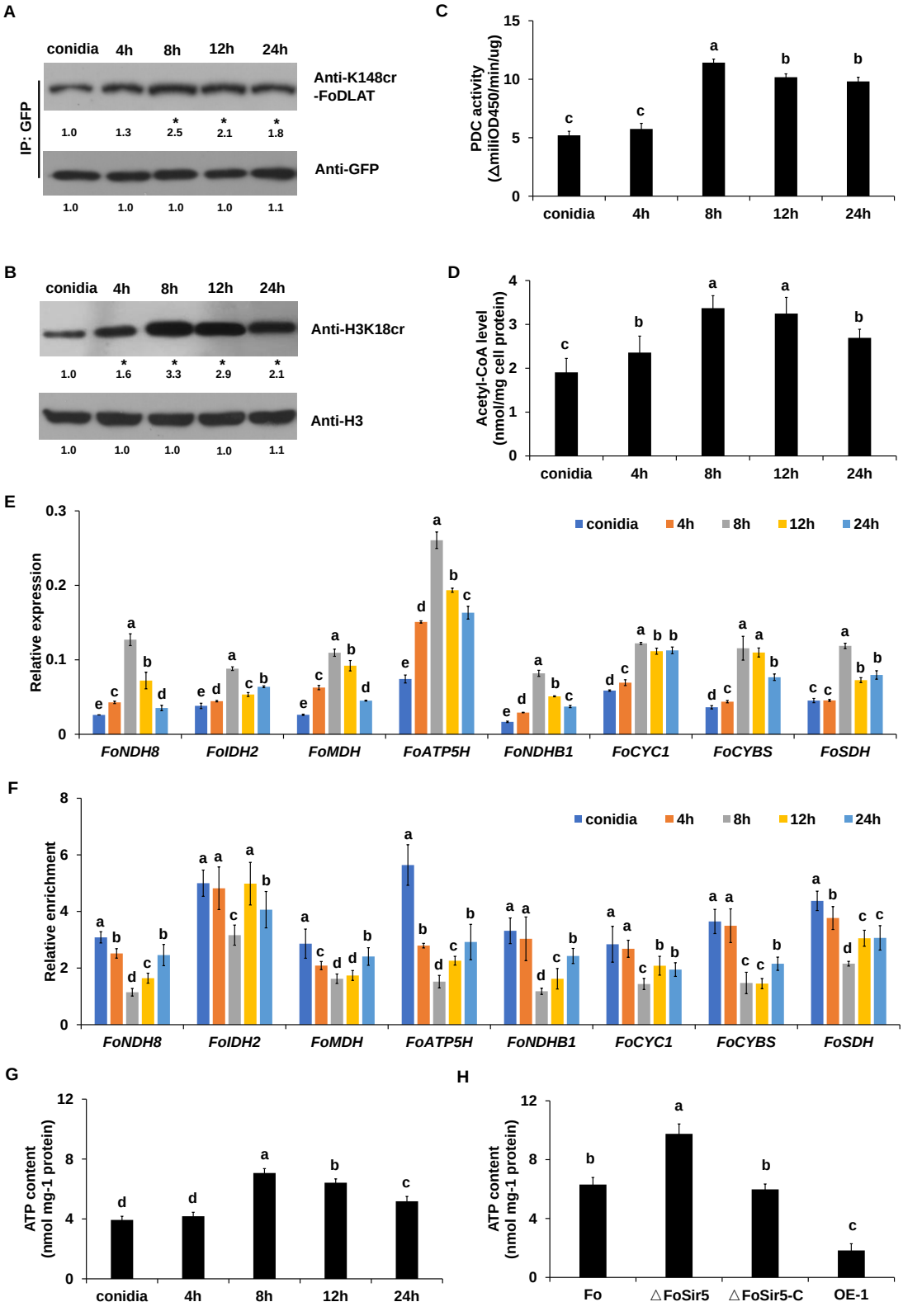

Figure 4. FoSir5 affects ATP production during gemination in *F. oxysporum*. **(A-B)** Western blot analysis showed the dynamic changes of FoDLAT K148 (A) and histone

H3K18 (B) crotonylation during germination using the indicated antibodies. Numbers below the blots represent the relative abundance of FoDLAT-K148cr or H3K18cr. Anti-GFP or anti-H3 immunoblotting was used to show equal loading, respectively. **(C-D)** PDC activity (C) and acetyl-CoA production (D) in *F. oxysporum* during germination were determined. **(E)** Expression profile of the aerobic respiration-related genes during the germination process. **(F)** Relative enrichment of the immunoprecipitated promoter regions in aerobic respiration-related genes during germination determined using anti-GFP antibody in the FoSir5-GFP strain driven by the native promoter. The fold enrichment was normalized to the input and internal control gene (*β-tubulin*). **(G)** ATP content of *F. oxysporum* during germination. **(H)** Effect of FoSir5 on the ATP content of the indicated strains, as determined in germinating conidia at 8 h post incubation (h.p.r.). The presence of different letters (A-H) above the mean values of three replicates indicates a significant difference between different samples ($P < 0.05$, ANOVA).

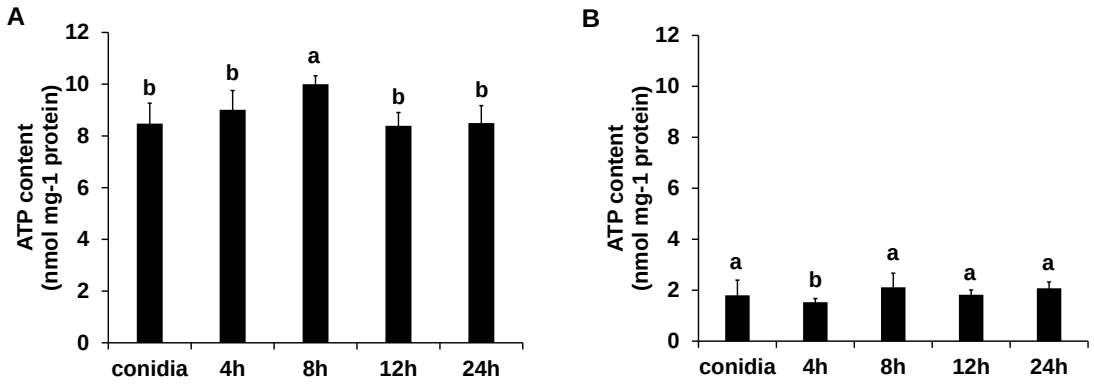

Figure 4-figure supplement 1. The ATP content of ΔFoSir5 mutant **(A)** and OE-1 strain **(B)** during germinating process. The presence of different letters above the mean values of three replicates indicates a significant difference between different samples ($P < 0.05$, ANOVA).

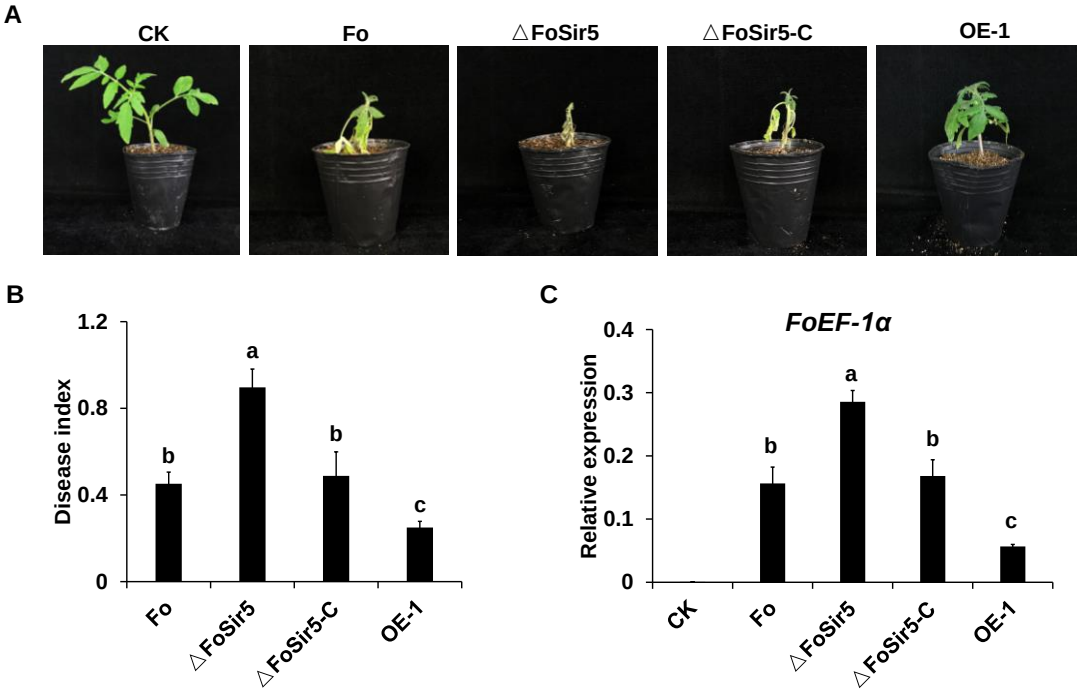

Figure 4-figure supplement 2. Impact of FoSir5 on the virulence of *F. oxysporum*. **(A)** Pathogenicity of the indicated strains in tomato after 8 days of incubation. **(B)** Quantification of the disease indexes of the indicated strains. **(C)** qRT-PCR analysis of *F. oxysporum EF-1α* transcript levels in tomato plants harvested 14 days after infection with the indicated strains. The expression of tomato *RCE1*, a constitutively expressed gene, was used as a control for the use of equal amounts of RNA for RT-PCR. The letters (B and C) above the mean values of three replicates indicate significant differences between different strains ($P < 0.05$, ANOVA).

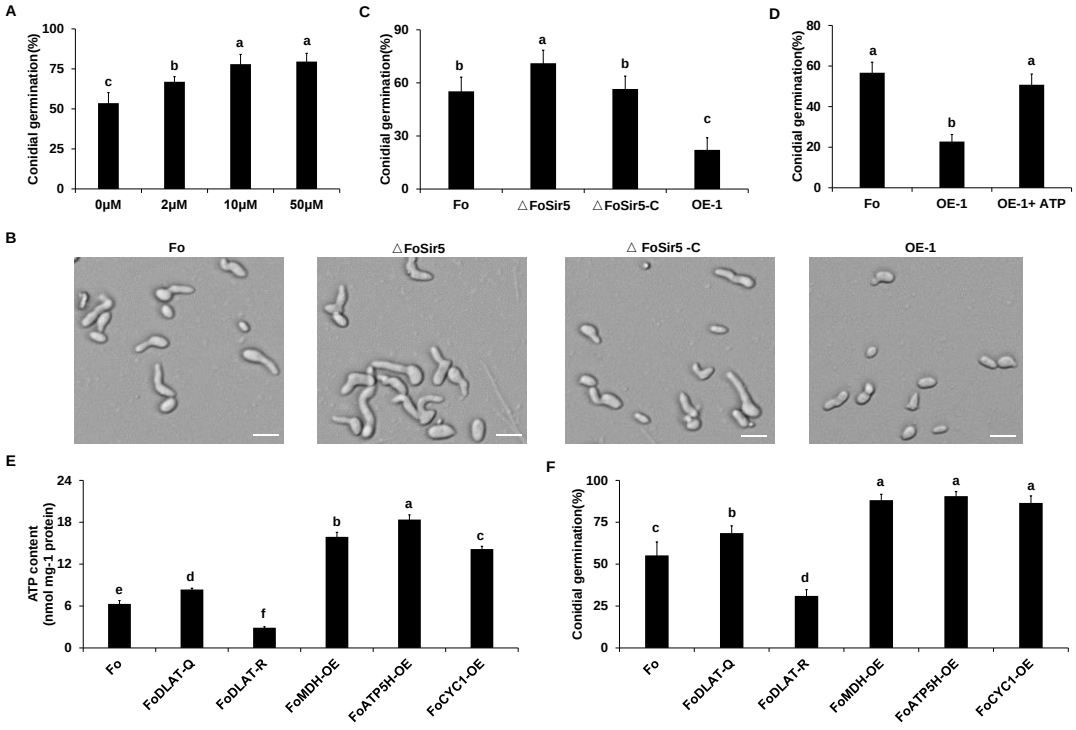

Figure 5. FoSir5 modulates conidial germination through affecting ATP synthesis. **(A)** Quantification of the conidial germination of *F. oxysporum* in PDB supplied with different concentrations of exogenous ATP at 8 h.p.r. **(B)** Conidial germination of the indicated strains in PDB on glass slides at 8 h.p.r. Representative images from three or more independent experiments, all of which had similar results. Scale bars = 30 μm. **(C)** Quantification of the conidial germination of the indicated strains in PDB on glass slides at 8 h.p.r. **(D)** Quantification of the conidial germination of the OE-1 strain with or without treatment with exogenous ATP at 8 h.p.r. **(E-F)** Effect of FoDLAT -K148Q/R mutations or overexpression of key genes of aerobic respiration on ATP production (E) and conidial germination (F) in *F. oxysporum*. The ATP content and germinating rate were determined at 8 h.p.r. The letters (A-F) above the mean values of three replicates indicate significant differences between different strains ($P < 0.05$, ANOVA).

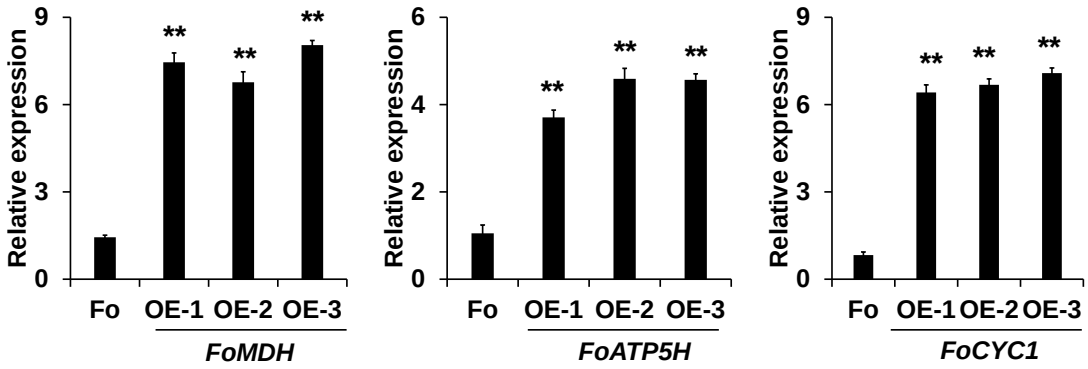

Figure 5-figure supplement 1. RT-PCR analysis of *FoMDH*-, *FoATP5H*-, and *FoCYC1*-overexpressing transformants. Data are the means ± SDs (n = 3); **P < 0.05 by unpaired two-tailed t-test.

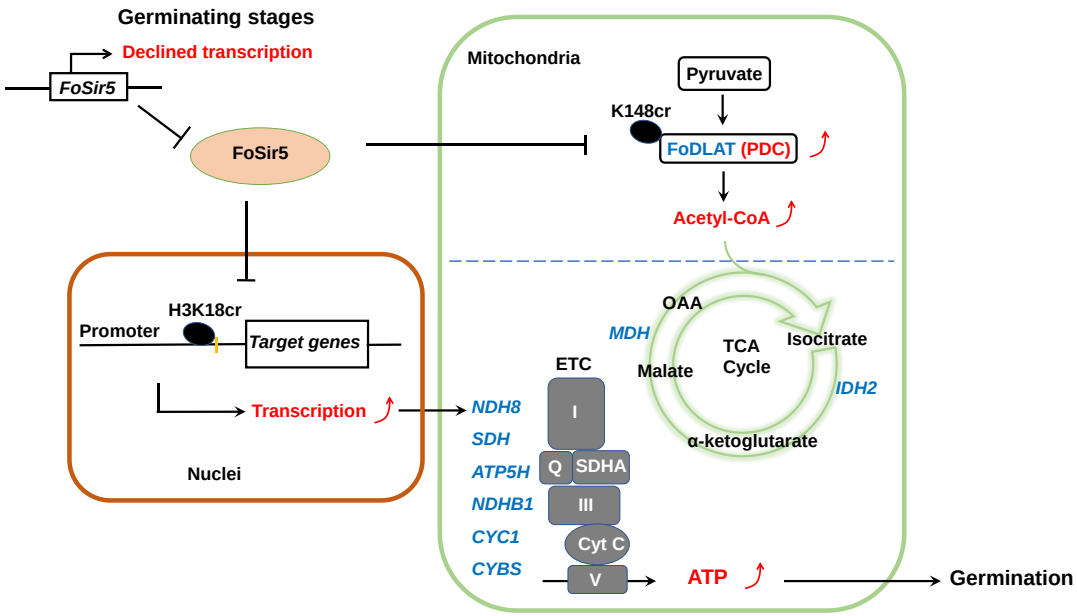

Figure 6. A model for FoSir5 functioning as a decrotonylase in different organelles to regulate conidial germination. During the germination process, the expression of *FoSir5* decreases, leading to relief of the inhibitory effect of FoSir5 on PDC activity through the decrotonylation of FoDLAT-K148cr and transcription of aerobic respiration-related genes by the reversal of H3K18cr. Thus, mitochondrial ATP biosynthesis is enhanced, promoting conidial germination in *F. oxysporum*.

Supplementary File 1. Putative FoSir5 interacting proteins

Supplementary File 2. RNA-seq gene expression data

Supplementary File 3. Primers used in the study

Figure legends for source data:

Figure 1- source data. Cellular localization and activity of FoSir5 in *F. oxysporum*. **(A)** Sirtuin proteins in *F. oxysporum* with predicted subcellular localizations. [a] Accession number of the full-length protein sequence available at Ensembl. [b] Localization of the *F. oxysporum* Sir2 protein determined by WoLF PSORT. **(B)** Phylogenetic tree relating FoSir5 to the orthologous human Sirtuin isoforms SIRT1 (NP_036370), SIRT2 (NP_085096), SIRT3 (NP_001357239), SIRT4 (NP_036372), SIRT5 (NP_001363737), SIRT6 (NP_057623), and SIRT7 (NP_057622). The tree is based on neighbour-joining analysis using MEGA-X. **(C)** Fluorescence microscopy analysis of FoSir5-GFP localization with MitoTracker Red (MT) and DAPI. Scale bars = 10 µm. **(D)** Subcellular fractionation of FoSir5-GFP transformants in *F. oxysporum*. Nuclear, cytoplasmic, and mitochondrial proteins were separately extracted and FoSir5-GFP were detected with anti-GFP antibody (Materials and Methods). The fractionation controls were ATP5A1 (mitochondria), Tubulin (cytosol), and histone H3 (nucleus). C, cytosol; N, nucleus; Mito, mitochondria. **(E)** *In vitro* Kcr assays with 50 µg of native CTH, 5 mM NAD^+ and 0.5 µg of FoSir5-His in the presence of 50, 100, or 200 µM crotonyl-CoA. Reaction materials were analyzed by Western blotting with anti-Kcr or anti-H3 antibody. Each scale bar represents the

mean ± SD for triplicate experiments. *indicates a significant difference between different pairs of samples ($P < 0.05$). **(F)** Expression profile of *FoSir5* in conidia, mycelium and during the germination process. The expression levels were normalized to that of the *F. oxysporum* elongation factor 1 alpha (EF-1α) gene. The presence of different letters above the mean values of three replicates indicates a significant difference between different samples ($P < 0.05$, ANOVA). (The red arrow indicates the original SDS–PAGE gels that were cropped for this panel.)

Figure 2- source data. FoSir5 decrotonylates FoDLAT, the E2 component of *F. oxysporum* pyruvate decarboxylase complex, with regulatory consequence. **(A)** Co-IP assays reveal physical interaction of FoSir5-GFP and FoDLAT-Flag. Western blot analysis of cell extracts from transformants co-expressing FoDLAT-Flag with GFP or FoSir5-GFP and elution from anti-GFP agarose. The fusion proteins were detected with anti-Flag or anti-GFP antibody. **(B)** *In vitro* pull-down assays to detect FoSir5-His with MBP or the FoDLAT-MBP fusion protein. FoDLAT-MBP was used as bait to pull down the FoSir5-His protein from the induced cell extracts. The MBP protein was assayed as a negative control. Input and bound forms of the pull-down fractions were detected with anti-His or anti-MBP antibody. **(C-D)** The K148 crotonylation (anti-K148cr-FoDLAT, top panel) and amount (anti-GFP, bottom panel) of FoDLAT-GFP and its mutant isoforms in the ΔFoSir5 (C) and OE-1 strain (D). Proteins were immunoprecipitated with anti-GFP antibody agarose beads and analyzed by anti-K148cr-FoDLAT or anti-GFP antibody. Representative gels are

shown from experiments carried out at least twice. Numbers below the blots represent the relative abundance of K148-crotonylated FoDLAT. Anti-GFP immunoblotting was used to show equal loading. **(E)** FoSir5 directly decrotonylates FoDLAT *in vitro*. Purified FoDLAT protein or its K148Q isoform (50 ng) were incubated with or without 50 ng of purified FoSir5 in the absence or presence of 5 mM NAD^+ and then analyzed by immunoblotting using anti-K148cr-FoDLAT or anti-His antibody. Each gel shown is representative of two experiments. Numbers below the blots represent the relative abundance of K148-crotonylated FoDLAT. Anti-MBP immunoblotting was used to show equal loading. **(F-G)** FoSir5 and K148 mutant FoDLAT affected PDC activity (F) and acetyl-CoA production (G) in *F. oxysporum*. PDC activity and acetyl-CoA production were determined in germinating conidia at 8 h. The presence of different letters above the mean values of three replicates indicates a significant difference between different strains ($P < 0.05$, ANOVA). (The red arrow indicates the original SDS–PAGE gels that were cropped for this panel.)

Figure 2-figure supplement 2- source data. Generation of targeted *FoSir5* gene deletion mutants and overexpression transformants. **(A)** Schematic representation of the targeted deletion of *FoSir5*. **(B)** PCR analysis of targeted deletion in the ΔFoSir5 strains. Genomic DNA was analyzed by PCR with the primer pairs indicated in panel (A). **(C-D)** RT-PCR (C) and WB (D) analysis of the FoSir5-Flag-overexpression transformants. Data of RT-PCR are the means ± SDs (n = 3); **$P < 0.05$ by unpaired two-tailed t-test. **(E)** Mycelial growth of the indicated strains on PDA plates after 3

1220 days of cultivation. (The red arrow indicates the original AGE or SDS–PAGE gels
1221 that were cropped for this panel.)
1222
1223 **Figure 2-figure supplement 3- source data.** Detection of crotonylation,
1224 succinylation, malonylation, and glutarylation on FoDLAT protein in ΔFoSir5
1225 compared with Fo. Proteins were immunoprecipitated with anti-GFP antibody agarose
1226 beads and analyzed by Western blot using the indicated antibodies. Representative
1227 gels are shown from experiments carried out at least twice. Anti-GFP immunoblotting
1228 was used to show equal loading. (The red arrow indicates the original SDS–PAGE
1229 gels that were cropped for this panel.)
1230
1231 **Figure 3- source data.** The downregulation of H3K18 crotonylation by FoSir5 and
1232 transcriptional repression of aerobic respiration-related genes. **(A)** Western blot
1233 analysis showed the effect of FoSir5 on histone H3K18 crotonylation and acetylation,
1234 and histone H3K9 crotonylation using the indicated antibodies. Numbers below the
1235 blots represent the relative abundance of different modifications. Anti-H3
1236 immunoblotting was used to show equal loading. **(B)** RNA-seq analysis of 8
1237 upregulated genes involved in aerobic respiration including *NDHB1* (NADH-quinone
1238 oxidoreductase chain B 1), *MDH* (malate dehydrogenase), *CYC1* (cytochrome C1),
1239 *IDH2* (isocitrate dehydrogenase subunit 2), *SDH* (succinate dehydrogenase), *ATP5H*
1240 (ATP synthase D chain), *NDH8* (NADH dehydrogenase iron-sulfur protein 8), and
1241 *CYBS* (succinate dehydrogenase cytochrome b small subunit). Differential expression

in three biological replicates illustrated using a heat map with coloured squares indicating the range of expression referred to as the FPKM value. **(C)** qRT-PCR validation of aerobic respiration-related genes in the indicated strains. The letters above the mean values of three replicates indicate significant differences between different strains ($P < 0.05$, ANOVA). **(D-E)** Relative enrichment of the immunoprecipitated promoter regions in aerobic respiration-related genes determined using anti-GFP antibody in the FoSir5-GFP strain and Fo strain containing GFP alone (D) or using anti-H3K18cr antibody in the Fo and ΔFoSir5 mutant strains (E). The fold enrichment was normalized to the input and internal control gene (*β-tubulin*). Data are the means ± SDs (n = 3); **$P < 0.05$ by unpaired two-tailed t-test. (The red arrow indicates the original SDS–PAGE gels that were cropped for this panel.)

Figure 4- source data. FoSir5 affects ATP production during gemination in *F. oxysporum*. **(A-B)** Western blot analysis showed the dynamic changes of FoDLAT K148 (A) and histone H3K18 (B) crotonylation during germination using the indicated antibodies. Numbers below the blots represent the relative abundance of FoDLAT-K148cr or H3K18cr. Anti-GFP or anti-H3 immunoblotting was used to show equal loading, respectively. **(C-D)** PDC activity (C) and acetyl-CoA production (D) in *F. oxysporum* during germination were determined. **(E)** Expression profile of the aerobic respiration-related genes during the germination process. **(F)** Relative enrichment of the immunoprecipitated promoter regions in aerobic respiration-related genes during germination determined using anti-GFP antibody in the FoSir5-GFP

strain driven by the native promoter. The fold enrichment was normalized to the input and internal control gene (*β-tubulin*). **(G)** ATP content of *F. oxysporum* during germination. **(H)** Effect of FoSir5 on the ATP content of the indicated strains, as determined in germinating conidia at 8 h post incubation (h.p.r.). The presence of different letters (A-H) above the mean values of three replicates indicates a significant difference between different samples ($P < 0.05$, ANOVA). (The red arrow indicates the original SDS–PAGE gels that were cropped for this panel.)